



Formation and impacts of nitryl chloride in Pearl River Delta

Haichao Wang^{1,4}, Bin Yuan^{2,3}, E Zheng^{2,3}, Xiaoxiao Zhang^{2,3}, Jie Wang¹, Keding Lu^{5,6}, Chenshuo Ye^{2,3},
Lei Yang^{2,3}, Shan Huang^{2,3}, Weiwei Hu⁷, Suxia Yang^{2,3}, Yuwen Peng^{2,3}, Jipeng Qi^{2,3}, Sihang Wang^{2,3},
Xianjun He^{2,3}, Yubin Chen^{2,3}, Tiange Li^{2,3}, Wenjie Wang^{2,8}, Yibo Huangfu^{2,3}, Xiaobing Li^{2,3},
Mingfu Cai^{2,3}, Xuemei Wang^{2,3}, and Min Shao^{2,3}

¹School of Atmospheric Sciences, Sun Yat-sen University, Zhuhai, 519082, China

²Institute for Environmental and Climate Research, Jinan University, Guangzhou, 511443, China

³Guangdong–Hong Kong–Macau Joint Laboratory of Collaborative Innovation for Environmental Quality,
Guangzhou, 511443, China

⁴Guangdong Provincial Observation and Research Station for Climate Environment and Air Quality Change in
the Pearl River Estuary, Key Laboratory of Tropical Atmosphere–Ocean System, Ministry of Education,
Southern Marine Science and Engineering Guangdong Laboratory (Zhuhai), Zhuhai, 519082, China

⁵State Key Joint Laboratory of Environmental Simulation and Pollution Control, College of Environmental
Sciences and Engineering, Peking University, Beijing, 100871, China

⁶The State Environmental Protection Key Laboratory of Atmospheric Ozone Pollution Control, College of
Environmental Sciences and Engineering, Peking University, Beijing, 100871, China

⁷State Key Laboratory of Organic Geochemistry and Guangdong Key Laboratory of Environmental
Protection and Resources Utilization, Guangzhou Institute of Geochemistry,
Chinese Academy of Sciences, Guangzhou 510640, China

⁸Multiphase Chemistry Department, Max Planck Institute for Chemistry, Mainz 55128, Germany

Correspondence: Bin Yuan (byuan@jnu.edu.cn)

Received: 6 June 2022 – Discussion started: 8 August 2022

Revised: 12 October 2022 – Accepted: 21 October 2022 – Published: 22 November 2022

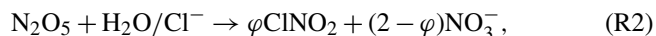
Abstract. Here we present a field measurement of ClNO₂ (nitryl chloride) and N₂O₅ (dinitrogen pentoxide) by a time-of-flight chemical ionization mass spectrometer (ToF-CIMS) with the Filter Inlet for Gas and AEROSols (FIGAERO) at a regional site in the Pearl River Delta during a photochemical pollution season from 26 September to 17 November 2019. Three patterns of air masses are sampled during this campaign, including the dominating air masses from the north and northeast urban regions (Type A), the southeast coast (Type B), and the South China Sea (Type C). The concentration of ClNO₂ and N₂O₅ was observed to be much higher in Type A and B than in Type C, indicating that the urban nighttime chemistry is more active than the background marine regions. The N₂O₅ uptake coefficient and ClNO₂ production yield were estimated based on the field measurement, and the performance of the previously derived parameterizations was assessed. The nighttime ClNO₂ correlated with particulate chloride and the mass concentration of fine particles (most likely due to aerosol surface area) suggested that the ClNO₂ formation was limited by the N₂O₅ uptake at this site. By examining the relationship between particulate chloride and other species, we implied that anthropogenic emissions (e.g., biomass burning) rather than sea salt particles dominate the origin of particulate chloride, although the site was only about 100 km away from the ocean. A box model with detailed chlorine chemistry is used to investigate the impacts of ClNO₂ chemistry on atmospheric oxidation. Model simulations showed that the chlorine radical liberated by ClNO₂ photolysis during the next day had a slight increase in concentrations of OH, HO₂, and RO₂ radicals, as well as minor contributions to RO₂ radical and O₃ formation (< 5 %, on daytime average), in all the three types of air masses. Relatively high contributions were observed in Type A and B. The overall low contributions of ClNO₂

to atmospheric oxidation are consistent with those reported recently from wintertime observations in China (including Shanghai, Beijing, Wangdu, and Mt. Tai). This may be attributed to the following: (1) relatively low particle mass concentration limited ClNO₂ formation; (2) other reactions channels, like nitrous acid (HONO), oxygenated volatile organic compounds (OVOCs, including formaldehyde), and ozone photolysis had a more significant radical formation rate during the ozone pollution episodes and weakened the ClNO₂ contribution indirectly. The results provided scientific insights into the role of nighttime chemistry in photochemical pollution under various scenarios in coastal areas.

1 Introduction

Chlorine radical is an important oxidant in the tropospheric besides OH radicals, NO₃ radicals, and ozone (Saiz-Lopez and von Glasow, 2012; Simpson et al., 2015; X. Wang et al., 2019), which alters the fate of many atmospheric compositions, including oxidants, reactive nitrogen compounds, volatile organic compounds (VOCs), and other halogens. The Cl radical is much more reactive than OH concerning certain VOCs (e.g., alkanes) by a few orders of magnitude for the reaction rate constant (Atkinson and Arey, 2003; Atkinson et al., 2006). Therefore it contributes to atmospheric oxidation capacity considerably in the troposphere despite low concentrations. For example, the global model showed about 20 % of ethane and 14 % of propane oxidation are attributed to chlorine chemistry at the global scale (X. Wang et al., 2019). Modeling simulations also demonstrated that chlorine chemistry enhanced oxidative degradation of VOCs by > 20 % at some locations (Sarwar et al., 2014).

Photolysis of ClNO₂ (Reaction R1) is a major source of the tropospheric chlorine radical (Thornton et al., 2010; Simpson et al., 2015); other chlorine radical sources include the reaction of HCl with OH (Riedel et al., 2012; Eger et al., 2019) and photolysis of Cl₂ and other halogen compounds like ICl and BrCl (Peng et al., 2021). Tropospheric ClNO₂ is not only a critical chlorine activation precursor but also a nocturnal reservoir of reactive nitrogen, which is mainly formed by N₂O₅ heterogeneous reaction on chlorine-containing particles with a branching ratio at nighttime (Reaction R2).



where φ represents the yield of ClNO₂. This mechanism was firstly proposed by Finlaysonpitts et al. (1989) through detecting the products of N₂O₅ uptake on NaCl particles. Given this reaction, the formation of ClNO₂ can be influenced by the N₂O₅ uptake (such as N₂O₅ uptake probabilities and aerosol surface area) as well as the production yield of ClNO₂.

The N₂O₅ uptake coefficient, $\gamma(\text{N}_2\text{O}_5)$, has been reported as highly varied under tropospheric conditions (Brown and Stutz, 2012). Both field and laboratory studies reveal that this process can be affected by ambient temperature, relative hu-

midity (Mozurkewich and Calvert, 1988; Mentel et al., 1999; Hallquist et al., 2003) and chemical compositions (such as the content of nitrate, liquid water, chloride, and organics) (Mentel et al., 1999; Brown et al., 2006; Bertram and Thornton, 2009; Gaston et al., 2014; McDuffie et al., 2018b; Tang et al., 2014; Anttila et al., 2006), as well as particle morphology (Mielke et al., 2013; Zong et al., 2021). Until now, the key factors that control N₂O₅ uptake coefficient in the different environments have not been well understood. ClNO₂ yield is also highly varied subject to the liquid water and chloride content in the aerosol (Behnke et al., 1997; Roberts et al., 2009; Bertram and Thornton, 2009). Several studies have demonstrated that the ClNO₂ yield is also affected by other factors like aerosol sulfate (Staudt et al., 2019) and organics (Ryder et al., 2015; Tham et al., 2018; McDuffie et al., 2018a). However, the comprehensive quantitative relationship of these factors in controlling the yield still has large uncertainties. These gaps in parameterization of N₂O₅ uptake coefficients and ClNO₂ yield result in being challenging to accurately predict ClNO₂ and particulate nitrate production.

Osthoff et al. (2008) and Thornton et al. (2010) directly observed elevated ClNO₂ in the coastal and inland US respectively by chemical ionization mass spectrometers (CIMSs). They have shed light on the significance of ClNO₂ photolysis in launching the radical chemistry during the morning time and also affecting halogen chemistry and reactive nitrogen cycling. Large amounts of chlorine radicals are liberated through the photolysis of nocturnal accumulated ClNO₂ (Reaction R1), which oxidizes VOCs and produces peroxy radicals (RO₂) to initiate the daytime radical cycling in the morning, when other radical sources, like ozonolysis and photolysis of O₃, HONO, and HCHO, are still weak (Osthoff et al., 2008). The impacts of ClNO₂ chemistry on the primary source of radicals and ozone formation comprise a critical topic, the answer to which is very helpful to narrow the gap of the missing primary source of RO_x and improve our knowledge of the current ozone pollution mechanism (Tan et al., 2017; Tham et al., 2016). Model simulation has highlighted ClNO₂ chemistry could increase mean daily maximum 8 h ozone by up to 7.0 ppbv in some areas in the Northern Hemisphere (Sarwar et al., 2014). The large contribution was also confirmed in the southern California region by a box model study (Riedel et al., 2014). In addi-

tion, global model simulation showed ClNO_2 chemistry increases wintertime ozone by up to 8 ppb over polluted continents (X. Wang et al., 2019). Particularly, previous modeling results have also highlight the importance of ClNO_2 chemistry in enhancing O_3 production in China (Li et al., 2016; X. Yang et al., 2022).

Several field studies have reported the measurement of ClNO_2 in varied environments in the past decade (Riedel et al., 2012; Young et al., 2012; Mielke et al., 2013; Riedel et al., 2013; Bannan et al., 2015; Faxon et al., 2015; Mielke et al., 2015; Phillips et al., 2016; Bannan et al., 2017; X. F. Wang et al., 2017; Z. Wang et al., 2017; Le Breton et al., 2018; McDuffie et al., 2018a; Yun et al., 2018a; Zhou et al., 2018; Bannan et al., 2019; Eger et al., 2019; Haskins et al., 2019; Jeong et al., 2019; Xia et al., 2020, 2021; Tham et al., 2016, 2014; Wang et al., 2016; Phillips et al., 2012; Lou et al., 2022; Sommariva et al., 2018), in which the maximum ClNO_2 up to sub-ppbv (parts per billion by volume) to several ppbv was reported, indicating its ubiquitous presence worldwide and a broad atmospheric impact over various regions. During the CalNex-LA campaign 2010, ClNO_2 was measured at a ground site, on a research vessel, and on an aircraft platform, which depicted a full picture of the abundance of ClNO_2 and confirmed its large impacts on atmospheric chemistry in both urban and coastal regions in California (Riedel et al., 2012; Young et al., 2012; Mielke et al., 2013). Recently, Wang et al. (2016) used a box model to simulate the chemical evolution of the plume after leaving the observation site in Hong Kong and showed ClNO_2 chemistry had a following-day enhancement of the ozone peak and daytime ozone production rate by 5%–16% and 11%–41%, along with a large increase of OH, HO_2 , and RO_2 concentration especially in the morning. While Xia et al. (2021) and Lou et al. (2022) reported winter measurements of ClNO_2 in northern and eastern China respectively, they both showed moderate ClNO_2 levels and relatively small contributions of ClNO_2 chemistry to radical source and ozone enhancement on campaign average. These results are quite different than those of the summertime in China (Tham et al., 2016; Wang et al., 2016; Tan et al., 2017) and highlight the large variation of ClNO_2 chemistry influenced by temporal spatial distribution.

Despite its likely importance to the regional atmospheric oxidation and air quality, investigations of ClNO_2 chemistry in China remain relatively sparse. There have been several field measurements of ClNO_2 conducted in China in recent years, but considering the large diversities of air mass in inland and coastal regions in China, more fieldwork and model works are needed to gain more insights into the ClNO_2 chemistry in various atmospheric environments and assess its atmospheric impacts. Until now, only a few field measurements of ClNO_2 have been reported in the Pearl River Delta (PRD) region (Tham et al., 2014; Wang et al., 2016; Yun et al., 2018a), and only Wang et al. (2016) reported a comprehensive analysis of the impact of ClNO_2 chemistry on radical

and ozone formation in 2013 as mentioned before. To understand the increasing O_3 problem in recent years (T. Wang et al., 2019) and examine the role of ClNO_2 chemistry in O_3 formation in PRD, we measured ClNO_2 , N_2O_5 , and other related parameters at a regional site in PRD during a severe photochemical pollution season in 2019. The abundance, formation, and variation during different air mass patterns are well characterized. The factors impacting its formation are diagnosed. Finally, the contribution of chlorine radicals liberated by ClNO_2 photolysis on the daytime radical chemistry, as well as ozone formation, is comprehensively assessed by a box model coupled with detailed chlorine chemistry.

2 Method

2.1 Measurement site

This campaign was conducted at the Guangdong Atmospheric Supersite of China, which is located on the top of a mountain (~ 60 m a.s.l.) in Heshan (22.728° N, 112.929° E), Jiangmen, Guangdong Province (S. Yang et al., 2022). This site was in the western Pearl River Delta with no major industries in the surroundings but with some farmland and a few residents living at the hill foot. The traffic is far away from this site and is believed to have little influence on the sampling. The anthropogenic activity is much lower than the urban regions like Guangzhou, but the air quality is often influenced by neighboring cities, especially the outflow of air masses from the regions in the north and northeast. Therefore, the air masses sampled at this site are sometimes representative of the urban pollution from the center of PRD. There were once many atmospheric intensive studies conducted on the site to study the air pollution in PRD (Tan et al., 2019; Yun et al., 2018b). In this study, the instruments were located on the top floor of the measurement building with inlets approximately 15 m above the ground. The data presented in the study were collected from 27 September to 17 November 2019, during which photochemical pollution occurred frequently (S. Yang et al., 2022). Time is given as CNST (Chinese national standard time = UTC+8 h). During the campaign, sunrise was approximately at 06:00 and sunset was approximately at 18:00 CNST.

2.2 Instrument setup

A comprehensive suite of instrumentation is overviewed and listed in Table 1. An iodide-adduct time-of-flight chemical ionization mass spectrometer (ToF-CIMS) with the Filter Inlet for Gas and AEROSols (FIGAERO) was applied to measure ClNO_2 and N_2O_5 along with other oxygenated organic species (Ye et al., 2021; Z. Wang et al., 2020). In brief, the gas-phase species were measured via a 2 m long, 6 mm outer-diameter polyfluoroalkoxy (PFA) inlet while the particles were simultaneously collected on a Teflon filter via a separate 2 m long, 10 mm outer-diameter copper tubing in-

let; both had flow rates of 2 L min^{-1} with a drainage flow of 20 L min^{-1} . The gas phase was measured for 25 min at 1 Hz, and the FIGAERO instrument was then switched to place the filter in front of the ion molecule region; it was then heated incrementally to $200 \text{ }^\circ\text{C}$ to desorb all the mass from the filter to be measured in the gas phase, which resulted in high-resolution thermograms. ClNO_2 and N_2O_5 are measured as the iodide-adduct ions at m/z 207.867 (IClNO_2^-) and m/z 234.886 (IN_2O_5^-) respectively in the ToF-CIMS. The measurement background and sensitivities for detecting ClNO_2 and N_2O_5 with the dependence of water content were quantified (see Appendix). The limit of detection (LOD) for ClNO_2 and N_2O_5 was 4.3 and 6.0 pptv in 1 min time resolution respectively, with an uncertainty of $\sim 30 \%$.

Sub-micron aerosol composition (PM_{10}) was measured by a high-resolution time-of-flight aerosol mass spectrometer (HR-ToF-AMS) (DeCarlo et al., 2006). The soluble ions of sodium and potassium were measured by a commercial instrument (GAC-IC) equipped with an aerosol collector and detected by ion chromatography (Dong et al., 2012). The particle number size distribution (PNSD) were measured by a scanning mobility particle sizer (SMPS, TSI 3938). The aerosol surface area was calculated based on the size distribution measurement and corrected to wet-particle state by a hygroscopicity growth factor, with a total uncertainty of determining wet aerosol surface areas of $\sim 30 \%$ (Liu et al., 2013). VOCs were measured by proton transfer reaction time-of-flight mass spectrometer (PTR-ToF-MS) (Wu et al., 2020; He et al., 2022) and an automated gas chromatograph equipped with a mass spectrometer or flame ionization detectors (GC-FID/MS). A commercial instrument (Thermo Electron model 42i) was used to monitor NO_x . O_3 was measured by a commercial instrument using ultraviolet (UV) absorption (Thermo Electron 49i). $\text{PM}_{2.5}$ was measured by a tapered element oscillating microbalance (TEOM, 1400A analyzer). SO_2 and CO were measured by commercial instruments (Thermo Electron 43i and 48i). In addition, the meteorological parameters were available during the measurement. Photolysis frequencies were determined by a spectroradiometer (Bohn et al., 2008). The aerosol liquid water content (ALWC) is calculated from the ISORROPIA-II thermodynamic equilibrium model (Clegg et al., 1998). We used the reverse mode in ISORROPIA-II with the input of water-soluble ions along with ambient temperature (T) and relative humidity (RH). Given the high RH in this campaign, we ran the model by assuming aerosol phases were metastable.

2.3 Box model setup

A zero-dimensional chemical box model constrained by the field campaign data was applied to simulate the ClNO_2 chemistry. The box model was based on the Regional Atmospheric Chemical Mechanism version 2 (RACM2) described in Goliff et al. (2013), and a chlorine-related chemical mechanism was added (H. Wang et al., 2017b; Tan et al., 2017).

Briefly, chlorine chemistry was adapted to RACM2 from the modifications to the Master Chemical Mechanism (Xue et al., 2015), and the oxidation products from reactions between lumped VOC species and chlorine radicals were adapted from those of OH oxidation from RACM2. $j(\text{ClNO}_2)$ was calculated according to the NASA Jet Propulsion Laboratory (JPL) recommendation based on the work by Ghosh et al. (2012). The impact of O_3 by ClNO_2 chemistry was assessed by differing the results of two scenarios with and without the constraints of the observed ClNO_2 in the model simulation. For the reaction rate constant of the lumped species with Cl, the fastest value from different species was used to represent the upper limit of the impact of chlorine chemistry. It should be noted that the setting will lead to over-estimation of the contributions from ClNO_2 chemistry. The model was constrained by the observed ClNO_2 , NO_x , O_3 , CO , VOCs (assignment to RACM2), photolysis frequencies, ambient temperature, and pressure. The model runs were from 29 September to 17 November 2019 with most of the measurement data accounted for and with a 2 d spin-up. The constant lifetime corresponds to a deposition velocity of 1.2 cm s^{-1} with an assumed boundary layer height of 1000 m used for the input trace gases, and the model-generated species were set to a 24 h lifetime due to the loss caused by the dry deposition (Lu et al., 2012). The input data were averaged and interpolated to 1 h resolution.

3 Results and discussions

3.1 Overview of measurement

Figure 1 shows the time series of ClNO_2 and relevant trace gases, particles, and meteorological parameters during the measurements. In this campaign, the meteorological condition featured a high temperature ($24.7 \pm 3.8 \text{ }^\circ\text{C}$), high humidity ($62.1 \pm 15.6 \%$), and low wind speed ($1.5 \pm 0.8 \text{ m s}^{-1}$), and the dominant airflow was from the north and northwest. Compared to previous measurements at the same site in January 2017 (Yun et al., 2018b), the temperature was higher and relative humidity was lower during the measurements. The average and maximum concentration of particulate matter ($\text{PM}_{2.5}$) was 47.6 ± 19.3 and $138 \mu\text{g m}^{-3}$ respectively, which is significantly lower than that observed in January 2017, with a maximum up to $400 \mu\text{g m}^{-3}$. The dominant air pollutant was O_3 with an hourly campaign maximum and average mean daily maximum 8 h O_3 (MDA8 O_3) of 152.8 and 75.2 ± 20.9 ppbv respectively. There was 27 d out of 53 d with the hourly maximum of O_3 exceeding the Chinese national air quality standard ($200 \mu\text{g m}^{-3}$, equivalent to 93 ppbv), suggesting severe ozone pollution during the measurement period in the PRD region. NO_2 concentration was also elevated with 21.0 ± 10.4 ppbv on campaign average. The concurrent high O_3 and NO_2 made large nitrate radical production rates occur with a daily average of 2.5 ± 2.1 ppbv h^{-1} (median,

Table 1. Summary of the information about observed gas and particle parameters during the campaign.

Species	Limit of detection	Methods	Accuracy
N ₂ O ₅	6.0 pptv (3σ, 1 min)	FIGAERO-ToF-CIMS	±30 %
ClNO ₂	4.3 pptv (3σ, 1 min)	FIGAERO-ToF-CIMS	±30 %
NO	60 pptv (2σ, 1 min)	Chemiluminescence	±20 %
NO ₂	0.3 ppbv (2σ, 1 min)	Catalytic convert	±20 %
O ₃	0.5 ppbv (2σ, 1 min)	UV photometry	±5 %
VOCs	0.1 ppbv (5 min)	PTR-ToF-MS	±30 %
VOCs	20–300 pptv (1 h)	GC-FID/MS	±20 %
PM _{2.5}	0.1 μg m ⁻³ (1 min)	TEOM	±5 %
CO	4 ppbv (5 min)	IR photometry	±5 %
SO ₂	0.1 ppbv (1 min)	Pulsed UV fluorescence	±10 %
HCHO	25 pptv (2 min)	Hantzsch fluorimetry	±5 %
PNSD	14–700 nm (4 min)	SMPS	±20 %
Aerosol composition	< 0.16 μg m ⁻³ (30 min)	GAC-IC	±30 %
PM ₁ components	0.15 μg m ⁻³ (4 min)	HR-ToF-AMS	±30 %
Photolysis frequencies	Varies with species (20 s)	Spectroradiometer	±10 %

1.8 ppbv h⁻¹). The campaign maximum NO₃ production rate was observed at up to 18.6 ppbv h⁻¹ in the afternoon on 11 November 2019. At night, the nitrate radical production rate was 1.8 ± 1.5 ppbv h⁻¹ on campaign average (median, 1.4 ppbv h⁻¹). However, the high NO₃ production rate did not mean high concentrations of NO₃, N₂O₅, and ClNO₂ in the atmosphere, as the concentration was affected by both their sources and their sinks.

N₂O₅ existed at a moderate concentration for most nights, with the daily nocturnal peaks ranging from < 100 to 1180 pptv and a nocturnal average of 64 ± 145 pptv. During the nights from 27–30 September 2019, the N₂O₅ concentration was significantly higher than other nights. The NO₃ lifetime, calculated by steady-state method (Brown et al., 2003), was much longer in those four nights than other nights, implying a relatively weak sink of NO₃–N₂O₅ for the first four nights. The lifetime of NO₃ was < 1 min in general (except the first four nights), indicating active NO₃ chemistry at this site. The NO₃ concentration was calculated assuming the thermal equilibrium of NO₂–NO₃–N₂O₅, with a possible lower bias caused by the equilibrium coefficient for reversible reactions of NO₃ and N₂O₅ (*K*_{eq}) (Chen et al., 2022). Figure 1 shows the variation in calculated NO₃ coincided with N₂O₅. Elevated NO₃ occurred on the first four nights with a maximum of 90 pptv (1 h time resolution), which is comparable with the reported NO₃ level at other sites in the Pearl River Delta (Wang and Lu, 2019; Brown et al., 2016). ClNO₂ showed a clear diurnal variation with high levels during the night. The nocturnal average and hourly maximum were 198 ± 232 and 1497 pptv respectively. The abundances of ClNO₂ and N₂O₅ are lower than those observed at the same site in 2017, with high N₂O₅ and the highest value ever observed of ClNO₂ of 3358 and 8324 pptv (1 min time resolution) respectively (Yun et al., 2018b). The difference in ClNO₂ levels between the two campaigns con-

ducted in 2017 and 2019 may be caused by the aerosol loading. High particulate chloride ion was observed in the site with 0.74 ± 1.33 μg m⁻³ on nocturnal average, which was higher at night with a peak in the second half of night and decrease in daytime.

3.2 Characterization of pollutants in different air masses

We noticed the air mass is highly varied during the measurements. For example, during the period of 2–5 October, the observed ozone and ClNO₂ were much lower than other days; while during the period of 11–13 November, the air masses were much polluted with high O₃, PM_{2.5}, and ClNO₂. We therefore plotted the backward trajectories of the 24 h history of air masses arriving at the measurement site at 500 m a.m.s.l. height at 00:00, 06:00, 12:00, and 18:00 day by day. The measurement period was separated into three patterns meteorologically according to the analysis of backward trajectories. Table 2 lists detailed information about the air mass classification. The air masses from the northeast (and north) were the dominant ones with a total of 37 d, which were characterized with the outflow of the center city clusters of PRD and those from inland through long-distance transport. We checked the pollutants of the air masses from PRD and north out of PRD (e.g., Hunan or Jiangxi Province), and no significant difference was found. Therefore, we merged the two inland air masses as Type A. The second type was coastal or offshore from the east and southeast (Type B), which features the outflow of coastal cities like Shenzhen and Hong Kong occurred on 12 d in total. The third type was clean air mass from the South China Sea (4 d, Type C). Figure 2 shows three cases of each air mass mentioned above.

The mean diurnal profiles of measured NO₂, O₃, N₂O₅, and ClNO₂; the particle chloride content; and the ratio of chloride to sodium in the three types of air masses are shown

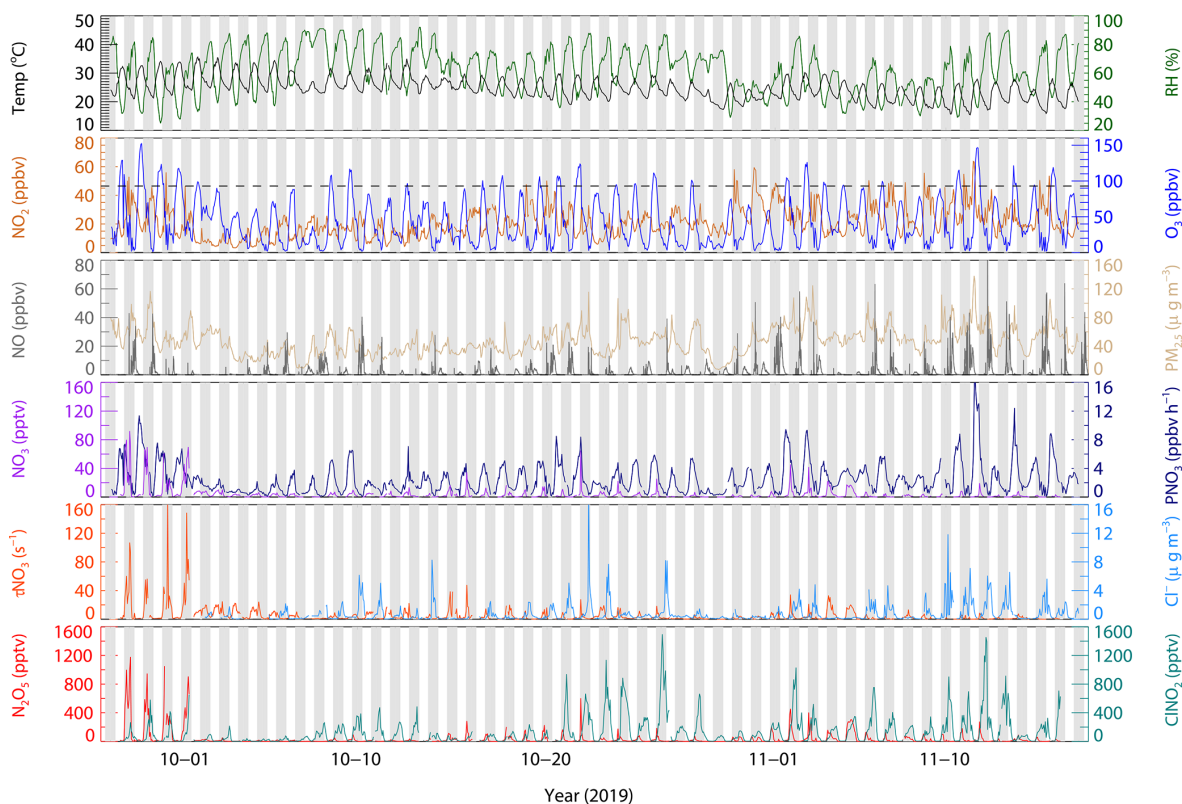


Figure 1. Time series of N_2O_5 , ClNO_2 , and relevant parameters. The dotted grey line in the O_3 panel denotes Chinese national air quality standard for hourly maximum O_3 ($200 \mu\text{g m}^{-3}$, equivalent to 93 ppbv). NO_3 radical is calculated based on a thermal equilibrium with measured NO_2 and N_2O_5 .

Table 2. The detailed information of three air mass types.

Air mass type	Periods	Days
Type A: inland air from northeast	26 September–1 October; 10 October; 11–20 October; 24 October–10 November; 14–15 November	37 (69.8 %)
Type B: coast air from east	6–7 October; 9–10 October; 21–23 October; 11–13 November; 16–17 November	12 (22.6 %)
Type C: marine air from south	2–5 October	4 (7.5 %)

in Fig. 3, with a detailed summary of related parameters in nocturnal medians listed in Table 3. High levels of NO_2 and O_3 were observed in Type A and B air masses, with a small difference of NO_2 diurnal variation during the second half of the night. In comparison, the two pollutants in type C were much lower. If we focus on the abundance at night, we find a large difference in the NO_2 level with a sequence Type A > Type B > Type C, which results in the same sequence of NO_3 productions in different air masses. The nocturnal NO_2 seems to be a good indicator of the level of pollution, and nocturnal CO , $\text{PM}_{2.5}$, and SO_2 also followed this order with highest concentration in Type A. These results in-

dicate that the most polluted air mass came from the inland urban regions of PRD.

Given the particulate chloride precursor of ClNO_2 , we examined its diurnal variations in the three air mass types. The highest level of Cl^- was found in Type B, followed by Type A and Type C (also at night). Although the diurnal profile of Cl^- in the three types is similar, the increasing rate of Cl^- during the second half of the night in Type A is much slower than those in coastal and offshore air masses. This implies a different source of chloride, which will be further discussed in Sect. 3.4. N_2O_5 was observed with moderate concentration in the Type A air mass throughout the night, with a nocturnal peak of 152.4 pptv between 20:00–

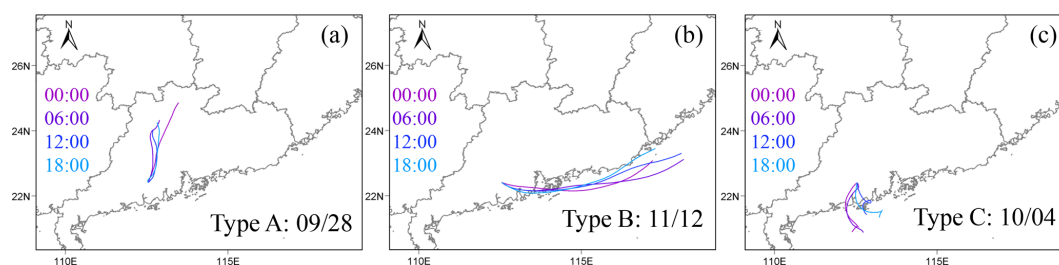


Figure 2. Three typical cases with air mass from different regions on 29 September, 12 November and 4 October respectively. Backward trajectory of 24 h history of air masses arriving at the measurement site with 500 m height at 00:00, 06:00, 12:00, and 18:00.

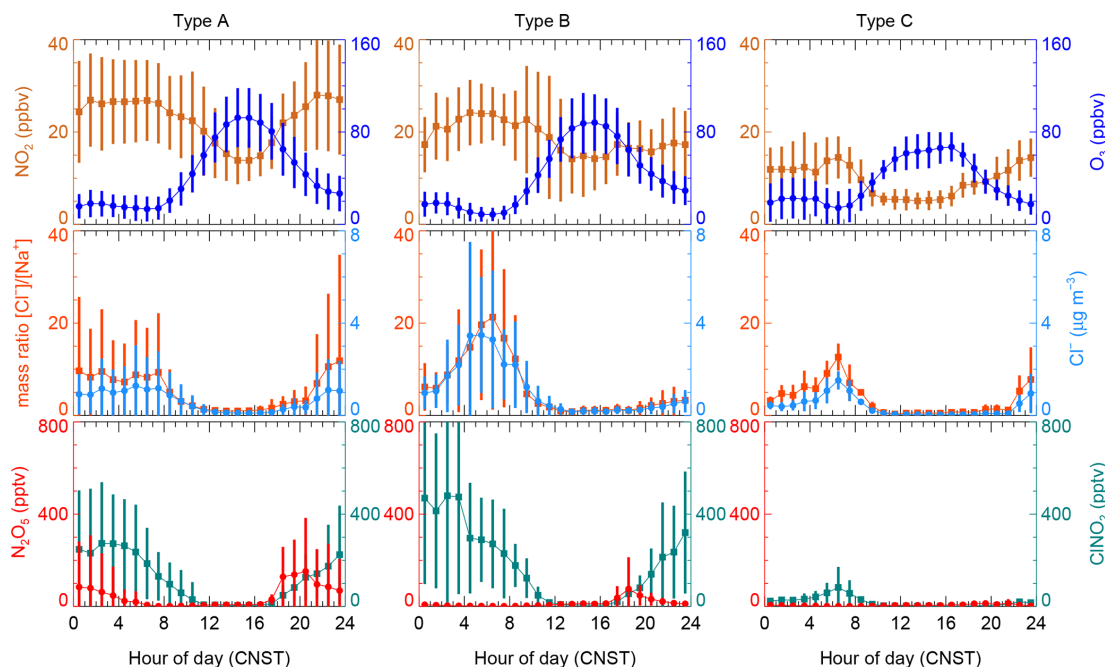


Figure 3. Mean diurnal profiles of N_2O_5 , ClNO_2 , and relevant parameters in the three types of air masses.

Table 3. Statistics results (median \pm standard deviation) of the related parameters in the three types of air masses (from 18:00 to 06:00 CNST).

Air mass	Type A	Type B	Type C
RH (%)	67.0 \pm 11.9	78.0 \pm 10.9	79.0 \pm 9.1
T ($^{\circ}\text{C}$)	22.8 \pm 3.0	23.3 \pm 2.2	25.6 \pm 1.9
ClNO_2 (pptv)	131.0 \pm 202.8	162.0 \pm 310.1	16.7 \pm 21.2
N_2O_5 (pptv)	17.8 \pm 164.9	6.3 \pm 64.6	2.8 \pm 9.3
Cl^- ($\mu\text{g m}^{-3}$)	0.41 \pm 1.11	0.56 \pm 1.85	0.33 \pm 0.51
$\text{PM}_{2.5}$ ($\mu\text{g m}^{-3}$)	53.0 \pm 18.8	41.0 \pm 21.8	32.0 \pm 10.2
SO_2 (ppbv)	5.0 \pm 4.7	3.4 \pm 11.4	3.4 \pm 4.7
Na^+ ($\mu\text{g m}^{-3}$)	0.12 \pm 0.07	0.18 \pm 0.09	0.09 \pm 0.03
$P(\text{NO}_3)$ (ppbv h^{-1})	1.60 \pm 1.49	1.39 \pm 1.50	0.69 \pm 0.49
NO_2 (ppbv)	24.8 \pm 10.9	18.1 \pm 6.2	11.2 \pm 5.8
O_3 (ppbv)	24.4 \pm 21.8	29.5 \pm 23.1	22.4 \pm 15.2
CO (ppbv)	540.3 \pm 122.3	448.4 \pm 130.7	367.5 \pm 89.8

21:00, while only a little N_2O_5 occurred in the first half of the night in Type B and C with a peak of 75.9 and 13.6 pptv respectively. The concentration difference may be attributed to two aspects. Firstly, the difference in $P(\text{NO}_3)$ results in more N_2O_5 produced in Type A. Secondly, compared with the air mass from coastal or offshore regions, the nocturnal temperature and RH condition from type A is much lower, and the loss of N_2O_5 may be faster in Type B and C than in Type A. The nocturnal median RH in Type A reached up to 67 %, while it reached 78 % and 79 % in Type B and Type C, suggesting a favorable condition for heterogeneous hydrolysis of N_2O_5 for all the three air mass types. The elevated ClNO_2 was observed in Type A and B with a nocturnal peak of 273.6 and 479.8 pptv respectively. Significantly less ClNO_2 was observed in the Type C air mass with a peak of 82.6 pptv. The reason for the different levels of ClNO_2 observed in the three air masses types is discussed in Sect. 3.4.

3.3 N₂O₅ uptake coefficient and ClNO₂ yield

In line with previous studies, we estimate the N₂O₅ uptake coefficient and ClNO₂ yield using the measurements of N₂O₅, ClNO₂, and particulate nitrate (Phillips et al., 2016; Wang et al., 2018; Tham et al., 2018). By assuming both the nocturnal enhancement of nitrate and ClNO₂ are mainly attributed to N₂O₅ uptake processes, ClNO₂ yield can be solely derived by the regression analysis of ClNO₂ versus particulate nitrate (Wagner et al., 2012; Riedel et al., 2013). The φ ClNO₂ can then be obtained by the fitted regression slope (S , Eq. 1) and named as the regression method.

$$\varphi = 2S/(S + 1) \quad (1)$$

Combining the data of N₂O₅ and aerosol surface area, the increase in ClNO₂ and nitrate can be simulated simultaneously by setting the input of the N₂O₅ uptake coefficient and ClNO₂ yield (named as the simulation method). The optimal N₂O₅ uptake coefficient and ClNO₂ yield are obtained simultaneously by adjusting the two parameters until the simulation reproduces the observed increase of ClNO₂ and nitrate (Phillips et al., 2016; Xia et al., 2020; Tham et al., 2018). This analysis assumes only the N₂O₅ uptake process dominates the increase of ClNO₂ and nitrate, and other physicochemical processes like vertical transportation and depositions are less important. This method requires the air mass in the analysis duration time to be relatively stable and less affected by emission and transportation. In addition, it is not valid in the case with negative changes of ClNO₂ and nitrate. The following selection criteria are set to pick out the suitable plumes to meet the assumptions. Firstly, the consistent increasing trends of ClNO₂ and NO₃⁻ and clear correlation between them during the analysis duration should be observed with a regression coefficient threshold of 0.5, which indicates the two products have the same source. Secondly, the increase in nitrate should be accompanied by an equivalent or faster increase in ammonium to ensure insignificant degassing of HNO₃ to the atmosphere. The observational data were averaged to 30 min for the following analysis; the time period of each derivation ranges from 2.5 to 10 h. Figure 4 depicts an example of the derivation on 5 November 2019, the stable S_a indicating a stable air mass during the analysis period. And the prediction reproduces well the observed increase in ClNO₂ and NO₃⁻.

During this campaign, we carefully identified 20 plumes with clear correlations between ClNO₂ and particulate nitrate by the slope method ($R^2 \geq 0.5$). As shown in Table 4, the derived ClNO₂ yield varied from 0.13 to 1.00 with a median of 0.45 ± 0.22 (mean value of 0.44). In the 20 plumes, we derived the N₂O₅ uptake coefficient and ClNO₂ for 12 cases in total. The results for the other eight nights were not valid due to the lack of S_a data (four nights), or unreasonably high results due to the observed low N₂O₅ concentration near the detection limit biased the simulations. We show good consistency of derived ClNO₂ yields by the two differ-

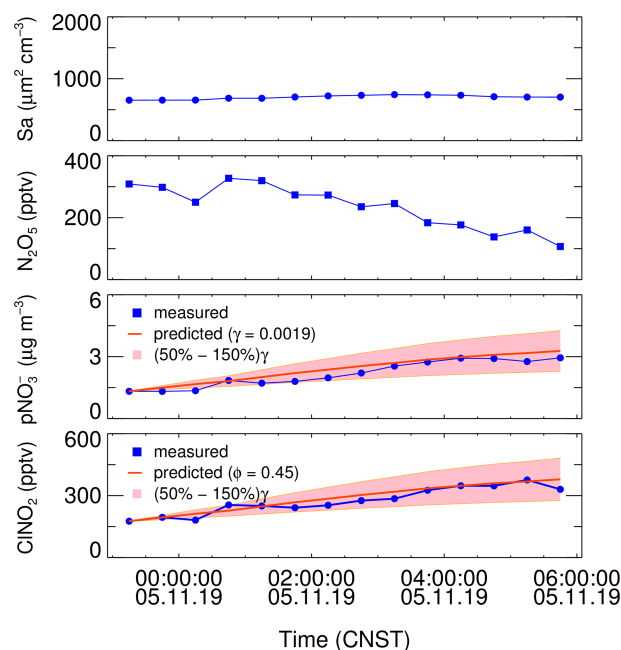


Figure 4. An example of the derivation of the N₂O₅ uptake coefficient and ClNO₂ yield constrained by observation of aerosol surface area, N₂O₅, and the enhancement of particulate nitrate and ClNO₂ on 5 November 2019. The pink region represents $\pm 50\%$ uncertainty of N₂O₅ uptake coefficient.

ent methods. The estimated N₂O₅ uptake coefficient showed a large variation and ranged from 0.0019 to 0.077 with a median of 0.0195 ± 0.0288 (mean value of 0.0317). The estimated γ N₂O₅ is within the range determined by previous field studies (Tham et al., 2018). Specifically in China, the average level of γ N₂O₅ is comparable with those reported in urban Beijing (H. Wang et al., 2017a, 2018), Wangdu (Tham et al., 2018), and Jinan (X. F. Wang et al., 2017) during the summertime but systematically higher than those determined in China in wintertime (Xia et al., 2021; H. Wang et al., 2020; Brown et al., 2016), except in the case reported on the urban canopy of Beijing (Chen et al., 2020). McDuffie et al. (2018a) summarized the reported φ ClNO₂ based on the observations, and we showed that the estimated average φ ClNO₂ in this study is at the middle to upper end of the values reported globally (Xia et al., 2021; McDuffie et al., 2018a). Due to the limited data points, we cannot distinguish the difference of γ N₂O₅ between the three air mass patterns. The ClNO₂ yields in Type A are slightly lower than those in Type B with an average of 0.41 and 0.47 respectively.

To gain insight into the factors governing the N₂O₅ uptake and ClNO₂ formation processes, the estimated γ N₂O₅ and φ ClNO₂ were compared with those predicted from complex laboratory-derived and field-derived parameterizations. An aqueous inorganic ionic reaction mechanism was once raised by Bertram and Thornton (2009) and established a volume-limited parameterization by considering the aerosol

Table 4. The derived N_2O_5 uptake coefficient and ClNO_2 yields at each night. NaN means not a number.

No.	Period	$\gamma\text{N}_2\text{O}_5^{\text{a}}$	$\varphi\text{ClNO}_2^{\text{a}}$	$\varphi\text{ClNO}_2^{\text{b}}$	$r^{2\text{b}}$	Type
1	2 October 01:00–06:00	NaN	NaN	0.13	0.90	C
2	2 October 23:00–06:00	NaN	NaN	0.25	0.90	C
3	11 October 01:00–04:00	NaN	NaN	0.65	1.00	B
4	14 October 23:00–04:00	0.017	0.28	0.23	0.56	A
5	18 October 18:00–21:00	0.0059	0.42	0.40	0.90	A
6	20 October 20:30–23:00	0.045	0.44	0.47	0.71	A
7	21 October 20:30–01:00	0.061	0.52	0.54	0.90	B
8	22 October 22:30–05:00	0.066	0.58	0.61	0.62	B
9	24 October 22:00–06:00	0.065	0.26	0.23	0.74	A
10	25 October 21:00–02:00	0.077	1.00	1.00	0.92	A
11	28 October 21:00–04:00	NaN	NaN	0.15	0.74	A
12	1 November 21:00–23:30	0.022	0.35	0.32	0.83	A
13	2 November 22:00–00:30	NaN	NaN	0.29	1.00	A
14	3 November 18:00–06:00	0.0031	0.52	0.50	0.92	A
15	4 November 22:00–06:00	0.0019	0.45	0.47	0.86	A
16	8 November 00:00–06:00	0.0097	0.34	0.32	0.85	A
17	10 November 00:00–04:00	NaN	NaN	0.59	0.80	A
18	11 November 22:00–04:00	NaN	NaN	0.53	0.50	B
19	12 November 22:00–04:00	NaN	NaN	0.42	0.62	B
20	13 November 21:00–00:00	0.0070	0.70	0.75	0.92	B

^a The values of $\gamma\text{N}_2\text{O}_5$ and φClNO_2 are derived by simulation method. ^b The φClNO_2 and the correlation coefficient (r^2) between ClNO_2 and particulate nitrate are derived by regression method; the data were filtered with a correlation coefficient obtained from linear fitting threshold of 0.5.

volume, surface area, nitrate content, ALWC, and chloride content (named BT09, Eq. 2).

$$\gamma_{\text{BT09}} = \frac{4H_{\text{aq}}Vk}{CS_{\text{a}}} \left(1 - \frac{1}{1 + \frac{k_3[\text{H}_2\text{O}]}{k_{2\text{b}}[\text{NO}_3^-]} + \frac{k_4[\text{Cl}^-]}{k_{2\text{b}}[\text{NO}_3^-]}} \right). \quad (2)$$

Here H_{aq} is Henry's law coefficient of N_2O_5 , V is the aerosol volume, k is equal to $1.15 \times 10^6 - (1.15 \times 10^6) \exp(-0.13[\text{H}_2\text{O}])$, $k_3/k_{2\text{b}}$ is the ratio of the reaction rate of H_2O versus NO_3^- to H_2ONO_2^+ that was set to 0.06, and $k_4/k_{2\text{b}}$ is the ratio of the reaction rate of Cl^- versus NO_3^- to H_2ONO_2^+ that was set to 29 (Bertram and Thornton, 2009). The mean values of the particulate-volume-to-surface ratio (V/S_{a}) were measured. A simple parameterization (EJ05) considering the effect of enhanced RH and temperature on the N_2O_5 uptake was also included (Evans and Jacob, 2005). In addition, the recently established empirical parameterization based on the same framework (named Yu20) optimized some parameters according to the meta-analysis of five field measurements in China by Yu et al. (2020), also assessed in the study. Figure 5a shows the correlation of estimated $\gamma\text{N}_2\text{O}_5$ versus the parameterization. All the three parameterizations fail to predict the high values. The simple parameterization of EJ05 had the best performance with a high correlation and a consistent prediction of the median value while the other two parameterizations, BT09 and Yu20, underestimated the observed $\gamma\text{N}_2\text{O}_5$. Figure 6a–h show the dependence of the observed $\gamma\text{N}_2\text{O}_5$ on the factors reported in previous literature

that possibly activated the processes of N_2O_5 uptake and ClNO_2 formation. We show that $\gamma\text{N}_2\text{O}_5$ is highly correlated with the ambient RH as well as liquid water content, confirming the critical role of water content in N_2O_5 uptake and explaining the reason why EJ05 had a good performance. The dependence of $\gamma\text{N}_2\text{O}_5$ on nitrate mass concentration does not follow the rule of nitrate suppressing effect (Wahner et al., 1998), which may be due to the covariance of the nitrate and liquid water content. With respect to other factors, insignificant impacts on the N_2O_5 uptake are obtained.

Bertram and Thornton (2009) also proposed a ClNO_2 yield parameterization method that considers the ratio of ALWC and chloride content (Eq. 3). Here, k_4/k_3 was the ratio of the reaction rate of H_2ONO_2^+ versus Cl^- to H_2O and adopted as 483 ± 175 . Behnke et al. (1997) determined a ratio of 836 ± 32 , while it is estimated to be 105 ± 37 in Yu et al. (2020).

$$\varphi_{\text{BT09}} = \left(\frac{[\text{H}_2\text{O}]}{1 + k_4/k_3[\text{Cl}^-]} \right)^{-1} \quad (3)$$

Figure 5b shows that all the predicted ClNO_2 yield based on the abovementioned parameterizations overestimated the observations. The performance of the parameterization schemes of BK97 and BT09 based on the model aerosol conditions, with an overestimation up to $\sim 100\%$, is expected and consistent with previous studies, which may be caused by the unaccounted for potentially competitive effect of other species like organics and sulfate for the NO_2^+ intermediate

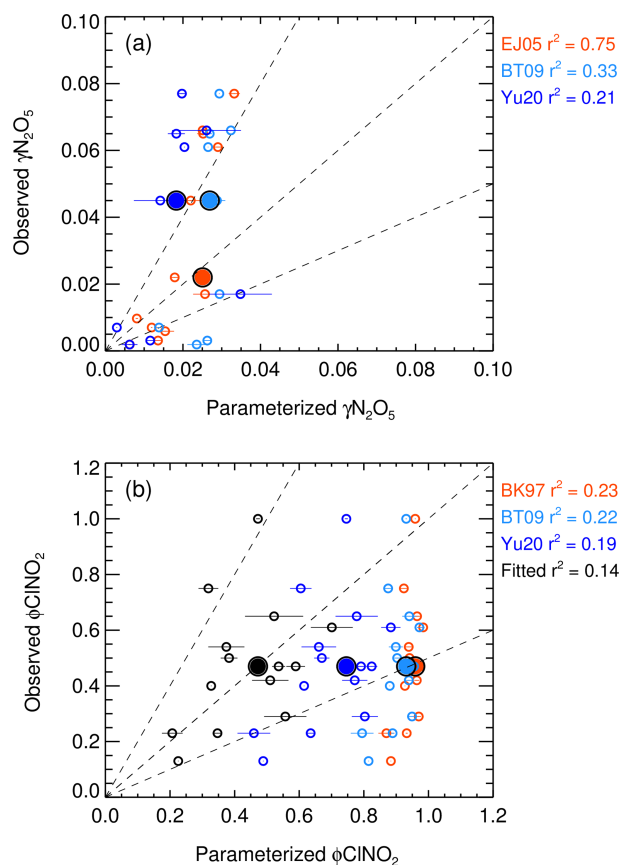


Figure 5. The inter-comparison of observation and parameterization of the N_2O_5 uptake coefficient (a) and ClNO_2 yield (b). The larger size of solid dots represents the median results. The parameterizations of EJ05, BT09, Yu20, and BK97 was cited from Evans and Jacob (2005), Bertram and Thornton (2009), Yu et al. (2020), Behnke et al. (1997) respectively. The fitted ClNO_2 yield (colored black) in panel (b) shows the best-fitting result in the study by adopting the k_4/k_3 of 32.0.

(McDuffie et al., 2018a; Staudt et al., 2019; Xia et al., 2021; Z. Wang et al., 2017). Although the empirical parameterization (Yu20) based on field observations improved the prediction and narrowed the gap effectively, the overestimation is still large with an average of $\sim 50\%$, which indicated that the yield is more strongly suppressed in this study than those observed in the campaigns of Yu et al. (2020). The factor 32.0 (k_4/k_3 in Eq. 3) was derived by iterative algorithms to achieve the best consistency between the observed and parameterized ClNO_2 yields, which is smaller than the Yu20 parameters by factors of 3.3. We examined the relationships of ClNO_2 yields with aerosol water content and other aerosol compositions as shown in Fig. 6i–p. We show that ϕ_{ClNO_2} only weakly correlated with the content of chloride (including the mass ratio and fraction in $\text{PM}_{2.5}$) and the molar ratio of chloride to water confirming the dependence found in laboratory studies. However, we did not find the dependence of the yields with aerosol organic or sulfate, as well as the RH

and water alone in the campaign, implying the ClNO_2 yield mechanism is much more complicated than the laboratory conditions.

3.4 The factors influencing ClNO_2 formation

The ClNO_2 formation can be largely affected by the budget of NO_3 – N_2O_5 and N_2O_5 uptake processes. The variation of NO_3 loss by VOC and NO activates the NO_3 loss distribution by N_2O_5 uptake and ClNO_2 formation indirectly. Figure 7 shows the correlation between the daily median ClNO_2 and mass concentration of chloride, $\text{PM}_{2.5}$, and the NO_3 production rate for the three types of air masses. Due to the limited dataset of Type C, the correlation analysis may not make sense; therefore, we did not take Type C into consideration in detailed discussion. We show that the mass concentration of chloride also showed a correlation coefficient with ClNO_2 by 0.66 and 0.31 for Type A and B respectively. Furthermore, the mass concentration of $\text{PM}_{2.5}$ correlated reasonably with the ClNO_2 formation with the correlation coefficient of 0.39 and 0.62 for Type A and B respectively. However, the levels of ClNO_2 demonstrate little relationship with the nitrate production rate. This is quite different from the results observed in the United Kingdom, where the ClNO_2 levels are mainly controlled by NO_2 and O_3 , rather than by the N_2O_5 uptake processes (Sommariva et al., 2018).

The low correlation between the ClNO_2 and NO_3 production rates is within expectations. In general, the production of nitrate radical controls the budget of N_2O_5 ; if N_2O_5 uptake dominated the sink of NO_3 , as a result, the N_2O_5 uptake and its products would show good correlation with NO_3 production rate. But in fact, NO_3 loss can also be affected by other loss pathways, like the reactions with NO and VOCs. In many cases, the NO_3 loss is dominated by VOC or NO, which means the ClNO_2 formation is suppressed. If the two loss pathways were highly varied due to irregular emissions, then the relationship between ClNO_2 and NO_3 production rate would be less correlated. We confirmed large variations of NO and VOC (not shown) on hourly and daily scales, which means the proportion of N_2O_5 uptake to the total loss of NO_3 is highly varied correspondingly. In addition, the variation of the N_2O_5 uptake coefficient and ClNO_2 yield also results in the weak correlation between the NO_3 production rate and ClNO_2 concentration. The weak correlation reflects the highly variable chemical processes from NO_3 production to ClNO_2 production in this region.

As the precursor of ClNO_2 , higher concentrations of particulate chloride result in high ClNO_2 yield from N_2O_5 uptake to some extent, as evidenced by our field observation (Fig. 6) and previous laboratory studies (Bertram and Thornton, 2009; Roberts et al., 2009; Ryder et al., 2015). High $\text{PM}_{2.5}$ concentrations usually provide more aerosol surface area to promote N_2O_5 uptake. The close relationship between ClNO_2 and $\text{PM}_{2.5}$ indicates that aerosol surface area is most likely a critical factor that limited ClNO_2 formation. The pro-

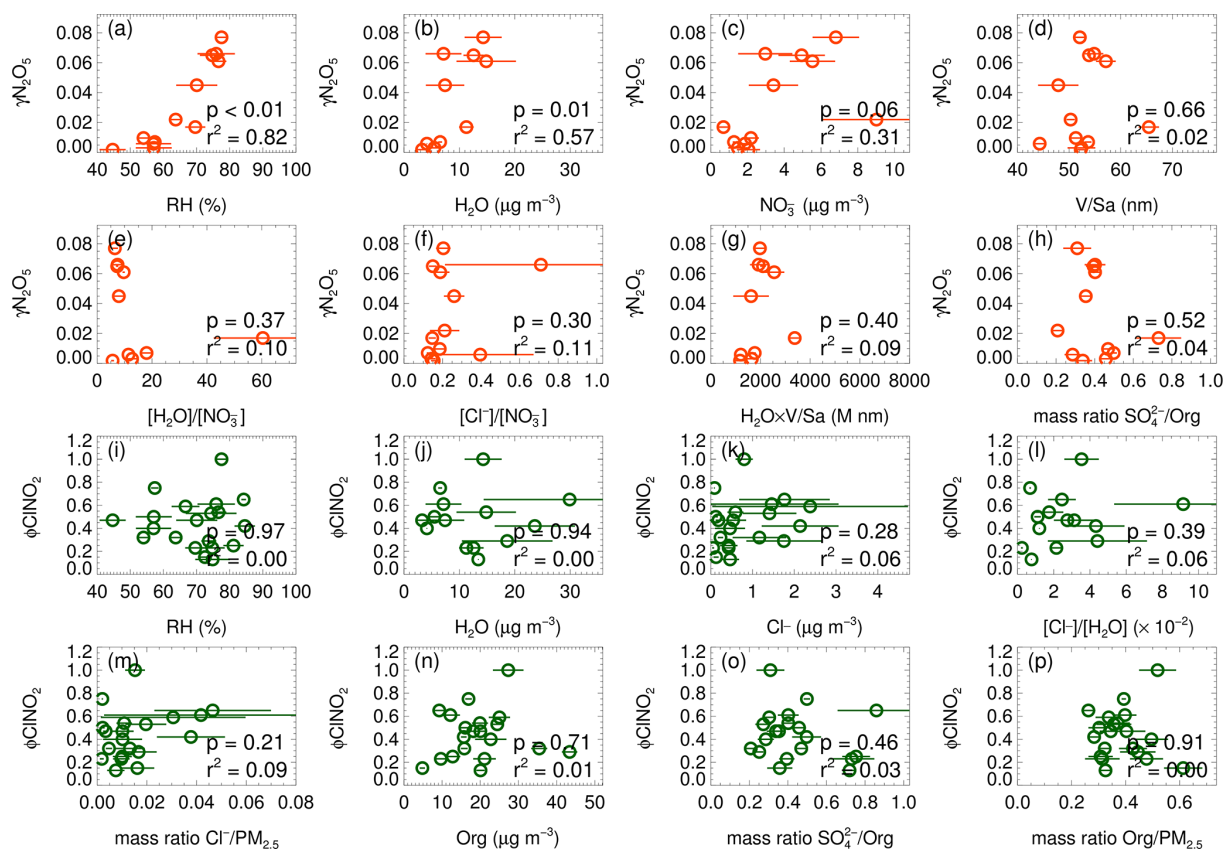


Figure 6. The estimated N_2O_5 uptake coefficient and ClNO_2 yield versus related parameters.

portion of nitrate in the total $\text{PM}_{1.0}$ was small with an average of 10.4 %; therefore the correlation of ClNO_2 and $\text{PM}_{2.5}$ cannot be attributed to the covariance between nitrate and $\text{PM}_{2.5}$. In addition, the ClNO_2 level in the air mass of Type B shows higher correlation to both Cl^- and $\text{PM}_{2.5}$ than Type A, suggesting that the ClNO_2 formation in type B is more effectively affected by the levels of chloride and $\text{PM}_{2.5}$.

Recent model simulations indicated that the ClNO_2 chemistry level is sensitive to the emission of chloride in the PRD (Li et al., 2021). In this study, a question raised is where is the source of chloride? The mass ratio of Cl^-/Na^+ is often used as an indicator of sea salt or anthropogenic sources to chloride with a threshold of 1.81 (Yang et al., 2018; Wang et al., 2016). A high ratio means the particulate chloride was affected by anthropogenic emission rather than sea salt. We determine that the mean mass ratios of Cl^- to Na^+ are 5.3, 6.3, and 3.1 in Type A, B, and C respectively (Fig. 3). This indicated that $\text{PM}_{2.5}$ sampled during the campaign was not strongly influenced by fresh sea salt aerosols. In the three types, the Type C air mass had the lowest ratio and may be influenced by both sea salt and anthropogenic emissions, which seems reasonable since it comes from the South China Sea. If we assume that the Type A air mass is free of sea salt and only influenced by anthropogenic activities, the higher ratio implies a more intensive chloride source in Type B. The cor-

relation between particulate chloride and some possible indicators, including K^+ , benzene, SO_2 , CO, and acetonitrile (CH_3CN) was examined day by day. Figure 8 shows the max correlation coefficient (R^2) on each day with a threshold of 0.5. We filtered out 39 out of 46 d during this campaign with a fraction of 85 %. Among the 39 d, a total of 11 d is associated with the strongest correlation between Cl^- and benzene, which typically come from industrial emissions. Cl^- also correlated with K^+ , CO, and CH_3CN in 19 d in total, implying potential contributions from biomass burning emissions. A total of 9 d for the highest correlations of Cl^- with SO_2 indicated coal-fired power plant emissions may also have contributed to Cl^- emission. We summarized that the source of chloride may be highly varied from different anthropogenic activities including biomass burning and industrial processes as well as coal-fired power plants. The statistics results in Table 5 suggest that the Cl^- in the air mass of Type A was affected by various sources, especially related to the sources associated with K^+ , benzene, and CH_3CN ; the Cl^- in Type B was mainly contributed by the similar source of CO, and type C was only affected by coal-fired power plants emissions. In addition, Fig. 8 showed that there are 2 d that the correlations between Cl^- and Na^+ exceeded the max of the selected anthropogenic factor matrix, indicating

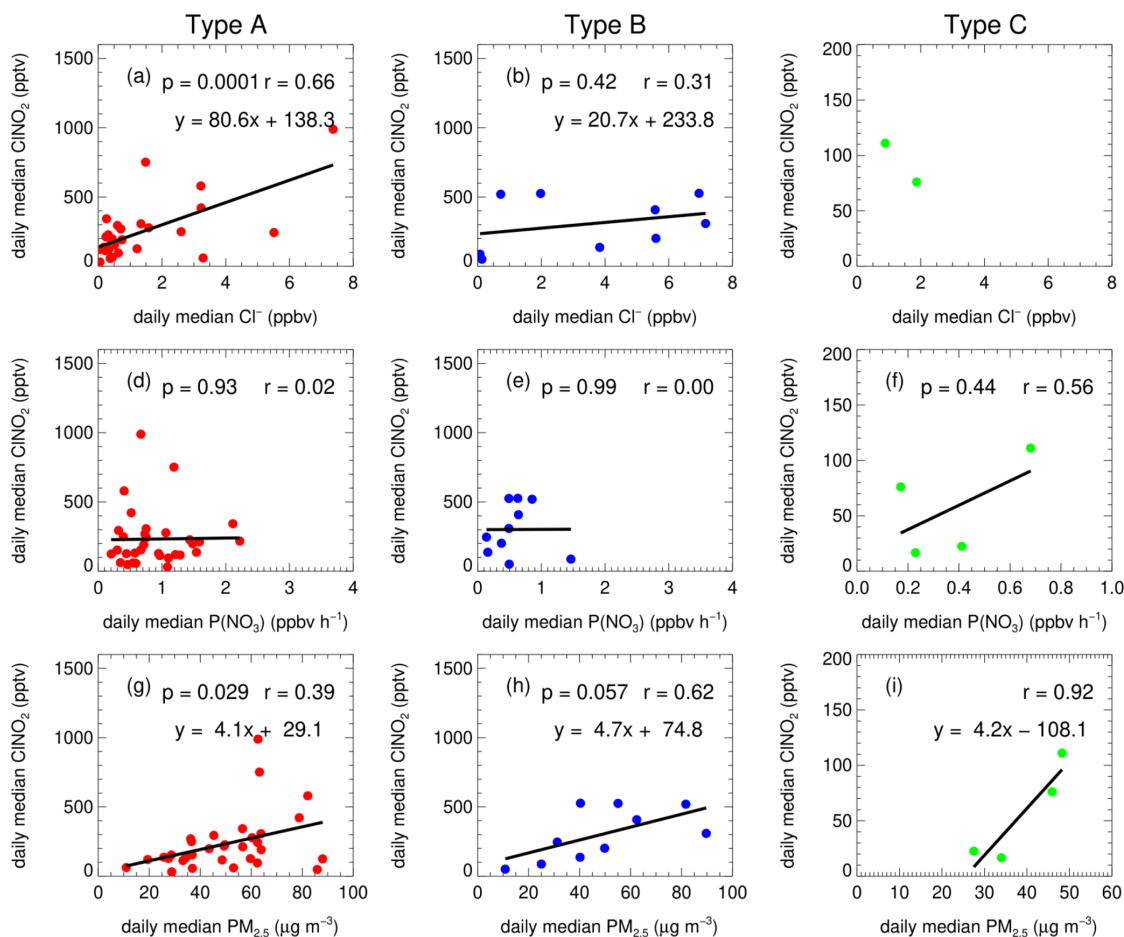


Figure 7. The functional dependence of the daily median of ClNO_2 on particulate chloride, nitrate radical production rate and $\text{PM}_{2.5}$ in the air mass of Type A (a, d, g), Type B (b, e, h), and Type C (c, f, i).

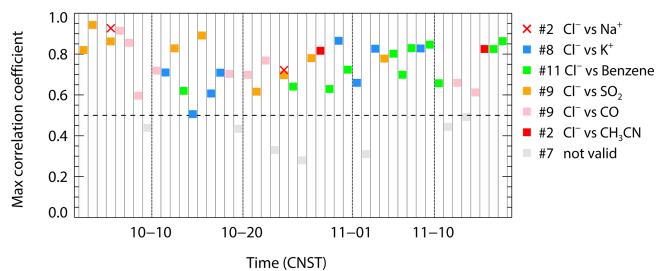


Figure 8. The max correlation coefficient between particulate chloride and a selected parameter matrix (including K^+ , benzene, SO_2 , CO, acetonitrile (CH_3CN)) on each day. The labeled number represents the days the event occurred; the dashed line denotes the threshold of 0.5 (39 valid days out of 46 in total). The cross means the correlation coefficient between Cl^- and Na^+ is larger than the max.

that the aerosol is still also impacted by sea salt to some extent.

Table 5. The statistics of the days for the highest factors correlated with particulate chloride in different air mass patterns.

Factors	Type A	Type B	Type C
K^+	8	0	0
Benzene	9	2	0
SO_2	5	1	3
CO	4	5	0
CH_3CN	2	0	0

3.5 The impacts of ClNO_2 on atmospheric oxidation

In this section, we focus on the assessment of the impact of ClNO_2 photolysis on the source of radicals and the contribution to the atmospheric oxidation. Figure 9 shows the diurnal accumulation of the RO_x production rate from model simulations with ClNO_2 chemistry in the three types of air mass. The total RO_x production rate was higher in Type A followed by Type B and C, in which photolysis of HONO, HCHO, O_3 , and OVOCs had large contributions. In addition, we noticed

the significant role of OVOCs (including photolysis and reaction with O_3) in producing RO_x at this site, especially in the Type A and B air mass. This result is consistent with that constrained by observed OVOCs in Guangzhou (W. Wang et al., 2022). The Cl radical, liberated by $CINO_2$, enhanced little RO_x production, with a morning peak contribution of 1.3 %, 2.2 %, and 1.8 % for Type A, B, and C, respectively (08:00–09:00). The contribution of $CINO_2$ photolysis to the production of RO_x is less than 1 % on daytime average, similar to the results obtained in winter Shanghai (Lou et al., 2022) as well as North China (Xia et al., 2021) and much lower compared to previous studies reported during the summertime in China (Tan et al., 2017; Tham et al., 2016). However, another winter campaign conducted in Hong Kong SAR in winter showed much more significant impacts compared to our observation (Wang et al., 2016), which indicated that the $CINO_2$ chemistry can also have a large influence on the radical formation in wintertime.

Figure 10 shows the enhancement of OH, HO_2 , and RO_2 radicals with the consideration of $CINO_2$ chemistry. The enhancement of the three radicals peaked in the morning. On average, OH concentration was enhanced by 1.5 % to 2.6 % in different air masses. The percentage of enhancement for the HO_2 radical was 1.9 % to 4.6 %, whereas the enhancement for RO_2 was a little bit higher (3.0 % to 6.8 %). In general, the enhancement of radicals was more significant in Type B than other two types of air masses, which is related to elevated $CINO_2$ concentrations for these air masses. Low $CINO_2$ and other radical precursors led to an earlier enhancement peak (08:00–09:00) in Type C and lasted a short time period. Although the increased peak occurred later at 09:00–10:00 for the air mass of Type A and Type B, the increase lasted for a longer time and had a longer effect. Overall, daytime OH, HO_2 , and RO_2 enhanced by 1.0 %, 2.0 %, and 3.0 % on campaign average.

Figure 11 depicts the integral enhancement of O_3 production by $CINO_2$ photolysis, which varied from less than 0.1 to 4 ppb day by day, with a percentage of < 1 % to 4.9 % with a median of 0.8 %. Our results are comparable with the winter case in North China (Xia et al., 2021). The next day, O_3 enhancement was highly correlated with the level of $CINO_2$ with a correlation coefficient of 0.7 (Fig. 11a). The daily net O_3 production was enhanced by 0.70 ppbv (0.9 %), 1.02 ppbv (1.9 %) and 0.24 ppbv (0.6 %) for daytime accumulation in Type A, B, and C respectively, which is consistent with the nocturnal level of $CINO_2$ in the three air masses presented in Table 3.

Table 6 summarized the observation-constrained box model simulation results about the impacts of $CINO_2$ chemistry. The average $CINO_2$ concentration in the observation is moderate compared with previous observations; other radical precursors (e.g., HCHO) were also elevated at the same time. This leads to a large total radical and ozone production rate and a relatively minor contribution by $CINO_2$ chemistry, which indicates that the contribution of $CINO_2$ chemistry is

affected by the budget of other radical precursors. In addition, significant contributions by $CINO_2$ chemistry to photochemical pollution were also frequently observed in different campaigns (Tham et al., 2016; Wang et al., 2016), in which the receptor site may have aging plumes with higher $CINO_2$ and thus larger contributions (Wang et al., 2016), suggesting the large variability of $CINO_2$ and its environmental impacts at various air masses. Here, our observations should be representative of the local condition and reflect the chemistry and impacts of $CINO_2$ on the air pollution in PRD region.

Previous studies suggest that chlorine radicals from $CINO_2$ photolysis may contribute significantly to the oxidation of some VOC species, especially for long-chain alkanes (Shi et al., 2020; K. Wang et al., 2022). The oxidation of long-chain alkanes (C_{10-14} n-alkanes) by chlorine and OH radicals during the morning hour (09:00–10:00) was also evaluated based on modeled oxidant concentration. We observed small contributions of the chlorine radical with a percentage of 4.3 %, 4.3 %, and 3.8 % for n-decane, n-dodecane, and n-tetradecane respectively, during the period (16 October to 17 November 2019) when the long-chain alkane measurement was valid. We also checked the role of chlorine radicals in short-chain alkanes oxidation, obtaining a slightly larger contribution than the long-chain alkanes, which is attributed to relatively large reaction rate constants between Cl and OH with respect to the short-chain alkanes. The daytime average contributions of Cl ranged from 1.4 %–1.6 % and varied by the chain length of the alkanes. Therefore, we concluded that chlorine radicals liberated by $CINO_2$ photolysis play a role in the oxidation of alkanes in the morning time but are not critical compared to OH oxidation on the daytime average. We note that several studies have reported that other sources produced a large number of halogen radicals like Cl_2 (Liu et al., 2017; Xia et al., 2020) and $BrCl$ (Peng et al., 2021) during the daytime reaction of HCl with OH (Riedel et al., 2012; Eger et al., 2019; Li et al., 2019). These may cause more alkanes oxidized by halogen radicals. However, it is not possible to assess the overall impacts by constraining all precursors of the chlorine radical in this work, which may warrant further investigation by more comprehensive field studies equipped with the instruments for detecting these species.

4 Conclusion

An intensive field study in the Pearl River Delta took place during a photochemical pollution season from 26 September to 17 November 2019, providing a comprehensive observation dataset to understand the $CINO_2$ chemistry and its impact on the air quality. We observed a wide variation for determining factors of $CINO_2$ formation in different kinds of air masses. Two types of air mass from northern and northeastern inland cities and the eastern coastal regions were polluted with elevated O_3 and related trace gases like NO_x and CO. Correlation analysis showed that $CINO_2$ formation

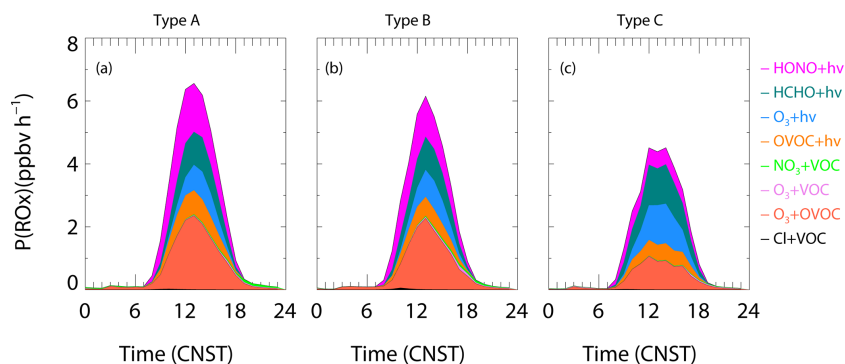


Figure 9. The diurnal cycle and distribution of RO_x production rate in the three types of air masses.

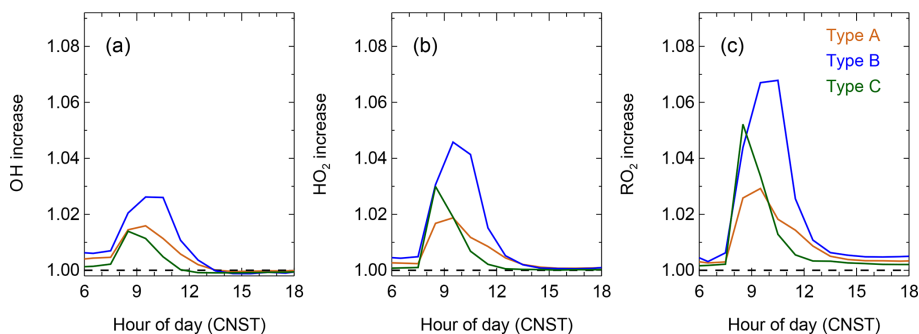


Figure 10. The diurnal cycle on the enhancement of OH (a), HO_2 (b), and RO_2 (c) by ClNO_2 chemistry in the three air mass patterns.

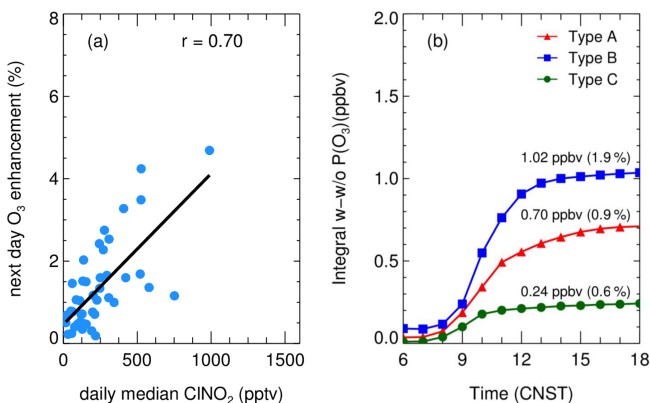


Figure 11. (a) The correlation of daily median ClNO_2 (18:00–06:00) and its impact on next-day net O_3 production enhancement during the campaign; (b) the average contribution of daytime integral O_3 by ClNO_2 mechanism in the three types of air masses.

is limited by chloride availability and $\text{PM}_{2.5}$ concentrations (mostly due to aerosol surface area) at this site.

We estimated the N_2O_5 uptake coefficients and ClNO_2 yield during this campaign and assessed the performance of previous parameterizations schemes. The newly developed observation-based empirical parameterization was also checked and showed an overall underestimation. We showed the $\gamma_{\text{N}_2\text{O}_5}$ only strongly correlated with RH, and the param-

eterization proposed by Evans and Jacob (2005) showed a considerable consistency with the observation. The ClNO_2 yield only showed weak correlation with the content of particle chloride, and the existing parameterizations systematically overestimated the yield. The particulate chloride mainly originated from anthropogenic emissions rather than sea salt. However, the specific contributing source of chloride in this region cannot be determined due to the varying correlation relationship with different kinds of anthropogenic emission indicators day by day. This result highlights the ClNO_2 chemistry may be triggered by many kinds of anthropogenic activities in the PRD regions (Wang et al., 2016; Yang et al., 2018).

The observation-constrained box model revealed chlorine radicals liberated by ClNO_2 chemistry had a relatively small contribution to the following daytime level of RO_x radicals and O_3 in this region. The small contribution of ClNO_2 chemistry in the PRD region may be due to the limited ClNO_2 produced by N_2O_5 uptake processes, and other strong primary sources of radicals weakened its contribution indirectly. Given the complex source of particulate chloride, we call for more field investigations to address the chlorine chemistry and its roles in air pollution in China.

Table 6. The summary of impacts of ClNO₂ on the next-day enhancement of ozone and radical production based on the box model that was constrained by field observations in previous literature.

Location	Duration	ClNO ₂ peak (ppbv)	Daytime average enhancement $P(O_3)$	Daytime average enhancement $P(RO_x)$	References
Heshan, CN	September–November 2019	1.5	1.0 %–4.9 %	< 2.2 %	this work
Shanghai, CN	October–November 2020	0.4	–	< 1.0 %	Lou et al. (2022)
Wangdu/Beijing/Mt. Tai, CN	2017–2018	1.7	1.3 %–6.2 %	1.3 %–3.8 %	Xia et al. (2021)
Wangdu, CN	June–July 2014	2.1	3.0 %	< 10.0 %	Tham et al. (2016)
Seoul, Korea	May–June 2016	2.5	1.0 %–2.0 %	–	Jeong et al. (2019)
Hong Kong, CN	November–December 2013	4.7	11.0 %–41.0 % ^a	–	Wang et al. (2016)
California, USA	May–June 2010	1.5	15.0 % ^b	17.0 %	Riedel et al. (2014)

^a Box model used to estimate the following evolution after the plume passing measurement site and the impacts on the next-day air quality. ^b Quantified the upper limit contribution to ozone pollution and RO_x formation.

Appendix A: The measurement background and calibration of CIMS

The background measurement of ClNO₂ and N₂O₅ was performed during the campaign. Figure A1 shows an example of the background check at the beginning of the campaign, which confirmed the negligible background signal in the measurement of ClNO₂ and N₂O₅ in the ambient condition. The calibration of ClNO₂ measurement sensitivity has been introduced in H. Wang et al. (2022). In brief, a nitrogen flow (6 mL min⁻¹) containing 10 ppmv Cl₂ was passed over a slurry containing NaNO₂ and NaCl to produce ClNO₂ (Thaler et al., 2011), and NaCl was included in the slurry in order to minimize the formation of NO₂ as a byproduct. The mixed flow containing ClNO₂ was then conditioned to a given RH and sampled into the CIMS instrument. To quantify ClNO₂, the mixed flow was delivered directly into a cavity attenuated phase shift spectroscopy instrument (CAPS, Model N500, Teledyne API) to measure background NO₂ concentrations or through a thermal dissociation tube at 365 °C to fully decompose ClNO₂ to NO₂, and the total NO₂ concentrations were then determined using CAPS. The differences in the measured NO₂ concentrations with and without thermal dissociation were equivalent to ClNO₂ concentrations. The CAPS instrument had a detection limit of 0.2 ppbv in 1 min for NO₂ and an uncertainty of ~ 10 %. To calibrate CIMS measurements of N₂O₅, a humidity-adjustable mixed flow containing stable N₂O₅, which was produced via O₃ oxidation of NO₂, was sampled into the CIMS instrument to obtain a normalized humidity dependence curve of N₂O₅. While the concentration of the N₂O₅ source is not quantified due to the absence of a N₂O₅ detector, we delivered the N₂O₅ source flow through a supersaturated sodium chloride solution to convert N₂O₅ to ClNO₂ with a unit efficiency at 50 % RH, which is a widely used method for the calibration of ClNO₂ by the CIMS technique. The absolute N₂O₅ sensitivity at 50 % RH can be realized and then scaled to other humidity conditions by the

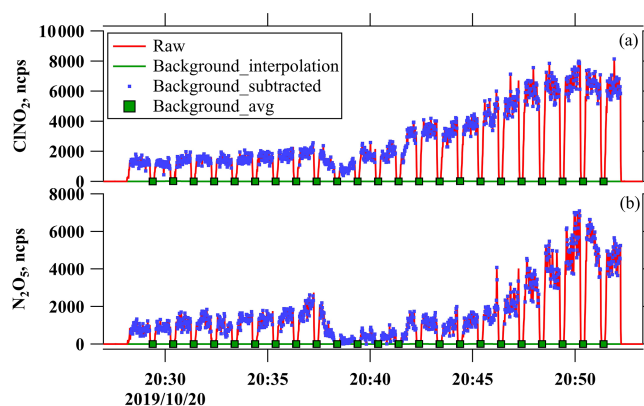


Figure A1. An example of background measurement for N₂O₅ (a) and ClNO₂ (b) on 20 October 2019.

normalized N₂O₅ sensitivity curve determined before. The sensitivity curves for N₂O₅ and ClNO₂ to water content are shown in Fig. A2. In this study, the sensitivity of the instrument was calibrated after the campaign. The main parameters (pressure, voltages, etc.) of the CIMS were checked every day and were relatively stable, indicating that the CIMS was operating stably during the campaign.

Figure A3 shows the high-resolution peak fitting results of typical mass spectra at m/z 235 and m/z 208 for N₂O₅ and ClNO₂ in three air mass patterns. The peaks of N₂O₅ and ClNO₂ were clearly resolved in the mass spectra. The peak of IN₂O₅⁻ can be well retrieved by separating a large adjacent peak of C₂H₄IO₃S⁻ in the air masses affected by marine emissions (Type B and C), which might be hydroperoxymethyl thioformate (HPMTF) from dimethyl sulfide oxidation (Veres et al., 2020). The interference signals including H₃INO₂S⁻ for ClNO₂ measurements can also be well separated in all the three air mass patterns. These results underline the necessity and feasibility in the application of the ToF analyzer in detecting N₂O₅ and ClNO₂ with an iodide CIMS.

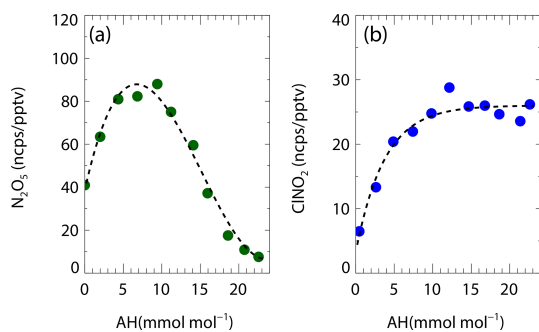


Figure A2. CIMS sensitivities as a function of absolute humidity (AH) for (a) N_2O_5 and (b) ClNO_2 .

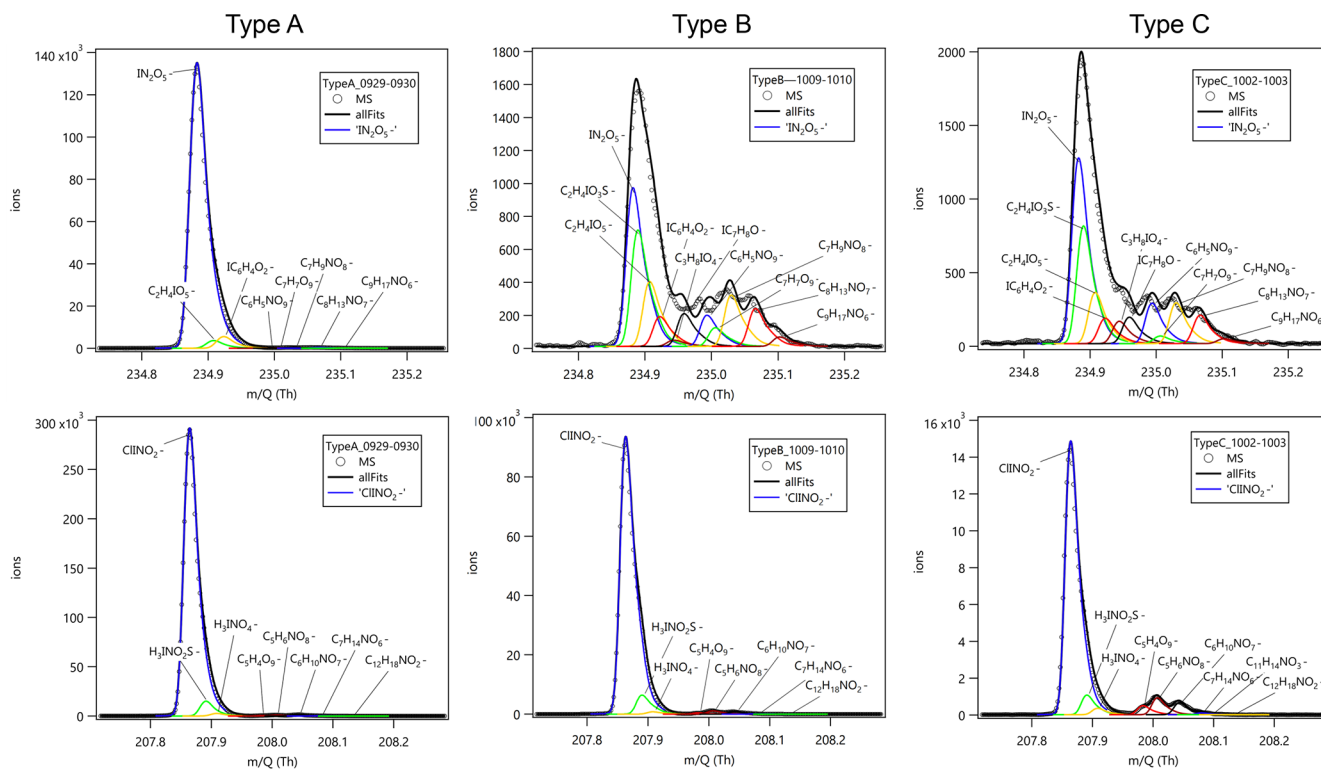


Figure A3. Cases of high-resolution spectra fitting for N_2O_5 and ClNO_2 by TOF-CIMS under three air mass patterns.

Code and data availability. The datasets and code used in this study are available from the corresponding author upon request (byuan@jnu.edu.cn).

Author contributions. HW and BY designed the study. EZ, XZ, JW and HW operated and calibrated the CIMS. KL, CY, LY, SH, WH, SY, YP, JQ, SW, XH, YC, TL, WW, YH, XL and MC conducted the field campaign and provided the sampling data. HW analyzed the data. HW and BY wrote the manuscript with inputs from all co-authors. XW and MS supervised the project.

Competing interests. The contact author has declared that none of the authors has any competing interests.

Disclaimer. Publisher's note: Copernicus Publications remains neutral with regard to jurisdictional claims in published maps and institutional affiliations.

Acknowledgements. The authors gratefully acknowledge the Jinan University science team for their technical support and discussions during this campaign. We thank for the NOAA Air Resources Laboratory for providing the HYSPLIT model.

Financial support. This research has been supported by the National Natural Science Foundation of China (grant nos. 41877302, 42175111, and 42121004), the Guangdong Innovative and Entrepreneurial Research Team Program (grant no. 2016ZT06N263), the Special Fund Project for Science and Technology Innovation Strategy of Guangdong Province (grant no. 2019B121205004), Guangdong Natural Science Funds for Distinguished Young Scholar (grant no. 2018B030306037), and Key Area Research and Development Program of Guangdong Province (grant no. 2019B110206001).

Review statement. This paper was edited by Timothy Bertram and reviewed by two anonymous referees.

References

- Anttila, T., Kiendler-Scharr, A., Tillmann, R., and Mentel, T. F.: On the reactive uptake of gaseous compounds by organic-coated aqueous aerosols: Theoretical analysis and application to the heterogeneous hydrolysis of N_2O_5 , *J. Phys. Chem. A*, 110, 10435–10443, <https://doi.org/10.1021/Jp062403c>, 2006.
- Atkinson, R. and Arey, J.: Atmospheric degradation of volatile organic compounds, *Chem. Rev.*, 103, 4605–4638, <https://doi.org/10.1021/cr0206420>, 2003.
- Atkinson, R., Baulch, D. L., Cox, R. A., Crowley, J. N., Hampson, R. F., Hynes, R. G., Jenkin, M. E., Rossi, M. J., Troe, J., and IUPAC Subcommittee: Evaluated kinetic and photochemical data for atmospheric chemistry: Volume II – gas phase reactions of organic species, *Atmos. Chem. Phys.*, 6, 3625–4055, <https://doi.org/10.5194/acp-6-3625-2006>, 2006.
- Bannan, T. J., Booth, A. M., Bacak, A., Muller, J. B. A., Leather, K. E., Le Breton, M., Jones, B., Young, D., Coe, H., Allan, J., Visser, S., Slowik, J. G., Furger, M., Prevot, A. S. H., Lee, J., Dunmore, R. E., Hopkins, J. R., Hamilton, J. F., Lewis, A. C., Whalley, L. K., Sharp, T., Stone, D., Heard, D. E., Fleming, Z. L., Leigh, R., Shallcross, D. E., and Percival, C. J.: The first UK measurements of nitryl chloride using a chemical ionization mass spectrometer in central London in the summer of 2012, and an investigation of the role of Cl atom oxidation, *J. Geophys. Res.-Atmos.*, 120, 5638–5657, <https://doi.org/10.1002/2014jd022629>, 2015.
- Bannan, T. J., Bacak, A., Le Breton, M., Flynn, M., Ouyang, B., McLeod, M., Jones, R., Malkin, T. L., Whalley, L. K., Heard, D. E., Bandy, B., Khan, M. A. H., Shallcross, D. E., and Percival, C. J.: Ground and Airborne UK Measurements of Nitryl Chloride: An Investigation of the Role of Cl Atom Oxidation at Weybourne Atmospheric Observatory, *J. Geophys. Res.-Atmos.*, 122, 11154–11165, <https://doi.org/10.1002/2017jd026624>, 2017.
- Bannan, T. J., Khan, M. A. H., Le Breton, M., Priestley, M., Worrall, S. D., Bacak, A., Marsden, N. A., Lowe, D., Pitt, J., Shallcross, D. E., and Percival, C. J.: A Large Source of Atomic Chlorine From ClNO_2 Photolysis at a UK Landfill Site, *Geophys. Res. Lett.*, 46, 8508–8516, <https://doi.org/10.1029/2019gl083764>, 2019.
- Behnke, W., George, C., Scheer, V., and Zetzsch, C.: Production and decay of ClNO_2 , from the reaction of gaseous N_2O_5 with NaCl solution: Bulk and aerosol experiments, *J. Geophys. Res.-Atmos.*, 102, 3795–3804, <https://doi.org/10.1029/96jd03057>, 1997.
- Bertram, T. H. and Thornton, J. A.: Toward a general parameterization of N_2O_5 reactivity on aqueous particles: the competing effects of particle liquid water, nitrate and chloride, *Atmos. Chem. Phys.*, 9, 8351–8363, <https://doi.org/10.5194/acp-9-8351-2009>, 2009.
- Bohn, B., Corlett, G. K., Gillmann, M., Sanghavi, S., Stange, G., Tensing, E., Vrekoussis, M., Bloss, W. J., Clapp, L. J., Kortner, M., Dorn, H.-P., Monks, P. S., Platt, U., Plass-Dülmer, C., Mihalopoulos, N., Heard, D. E., Clemitshaw, K. C., Meixner, F. X., Prevot, A. S. H., and Schmitt, R.: Photolysis frequency measurement techniques: results of a comparison within the ACCENT project, *Atmos. Chem. Phys.*, 8, 5373–5391, <https://doi.org/10.5194/acp-8-5373-2008>, 2008.
- Brown, S. S. and Stutz, J.: Nighttime radical observations and chemistry, *Chem. Soc. Rev.*, 41, 6405–6447, <https://doi.org/10.1039/C2cs35181a>, 2012.
- Brown, S. S., Stark, H., and Ravishankara, A. R.: Applicability of the steady state approximation to the interpretation of atmospheric observations of NO_3 and N_2O_5 , *J. Geophys. Res.-Atmos.*, 108, 4539, <https://doi.org/10.1029/2003jd003407>, 2003.
- Brown, S. S., Ryerson, T. B., Wollny, A. G., Brock, C. A., Peltier, R., Sullivan, A. P., Weber, R. J., Dube, W. P., Trainer, M., Meagher, J. F., Fehsenfeld, F. C., and Ravishankara, A. R.: Variability in nocturnal nitrogen oxide processing and its role in regional air quality, *Science*, 311, 67–70, <https://doi.org/10.1126/science.1120120>, 2006.
- Brown, S. S., Dube, W. P., Tham, Y. J., Zha, Q. Z., Xue, L. K., Poon, S., Wang, Z., Blake, D. R., Tsui, W., Parrish, D. D., and Wang, T.: Nighttime chemistry at a high altitude site

- above Hong Kong, *J. Geophys. Res.-Atmos.*, 121, 2457–2475, <https://doi.org/10.1002/2015jd024566>, 2016.
- Chen, X., Wang, H., Lu, K., Li, C., Zhai, T., Tan, Z., Ma, X., Yang, X., Liu, Y., Chen, S., Dong, H., Li, X., Wu, Z., Hu, M., Zeng, L., and Zhang, Y.: Field Determination of Nitrate Formation Pathway in Winter Beijing, *Environ. Sci. Technol.*, 54, 9243–9253, <https://doi.org/10.1021/acs.est.0c00972>, 2020.
- Chen, X., Wang, H., and Lu, K.: Interpretation of $\text{NO}_3\text{-N}_2\text{O}_5$ observation via steady state in high-aerosol air mass: the impact of equilibrium coefficient in ambient conditions, *Atmos. Chem. Phys.*, 22, 3525–3533, <https://doi.org/10.5194/acp-22-3525-2022>, 2022.
- Clegg, S. L., Brimblecombe, P., and Wexler, A. S.: Thermodynamic model of the system $\text{H}^+\text{-NH}_4^+\text{-SO}_4^{2-}\text{-NO}_3^-\text{-H}_2\text{O}$ at tropospheric temperatures, *J. Phys. Chem. A*, 102, 2137–2154, <https://doi.org/10.1021/jp973042r>, 1998.
- DeCarlo, P. F., Kimmel, J. R., Trimborn, A., Northway, M. J., Jayne, J. T., Aiken, A. C., Gonin, M., Fuhrer, K., Horvath, T., Docherty, K. S., Worsnop, D. R., and Jimenez, J. L.: Field-deployable, high-resolution, time-of-flight aerosol mass spectrometer, *Anal. Chem.*, 78, 8281–8289, <https://doi.org/10.1021/ac061249n>, 2006.
- Dong, H.-B., Zeng, L.-M., Hu, M., Wu, Y.-S., Zhang, Y.-H., Slanina, J., Zheng, M., Wang, Z.-F., and Jansen, R.: Technical Note: The application of an improved gas and aerosol collector for ambient air pollutants in China, *Atmos. Chem. Phys.*, 12, 10519–10533, <https://doi.org/10.5194/acp-12-10519-2012>, 2012.
- Eger, P. G., Friedrich, N., Schuladen, J., Shenolikar, J., Fischer, H., Tadic, I., Harder, H., Martinez, M., Rohloff, R., Tauer, S., Drewnick, F., Fachinger, F., Brooks, J., Darbyshire, E., Sciare, J., Pikridas, M., Lelieveld, J., and Crowley, J. N.: Shipborne measurements of ClNO_2 in the Mediterranean Sea and around the Arabian Peninsula during summer, *Atmos. Chem. Phys.*, 19, 12121–12140, <https://doi.org/10.5194/acp-19-12121-2019>, 2019.
- Evans, M. J. and Jacob, D. J.: Impact of new laboratory studies of N_2O_5 hydrolysis on global model budgets of tropospheric nitrogen oxides, ozone, and OH, *Geophys. Res. Lett.*, 32, L09813, <https://doi.org/10.1029/2005gl022469>, 2005.
- Faxon, C. B., Bean, J. K., and Hildebrandt Ruiz, L.: Inland Concentrations of Cl_2 and ClNO_2 in Southeast Texas Suggest Chlorine Chemistry Significantly Contributes to Atmospheric Reactivity, *Atmosphere*, 6, 1487–1506, <https://doi.org/10.3390/atmos6101487>, 2015.
- Finlaysonpitts, B. J., Ezell, M. J., and Pitts, J. N.: Formation of Chemically Active Chlorine Compounds by Reactions of Atmospheric NaCl Particles with Gaseous N_2O_5 and ClNO_2 , *Nature*, 337, 241–244, <https://doi.org/10.1038/337241a0>, 1989.
- Gaston, C. J., Thornton, J. A., and Ng, N. L.: Reactive uptake of N_2O_5 to internally mixed inorganic and organic particles: the role of organic carbon oxidation state and inferred organic phase separations, *Atmos. Chem. Phys.*, 14, 5693–5707, <https://doi.org/10.5194/acp-14-5693-2014>, 2014.
- Ghosh, B., Papanastasiou, D. K., Talukdar, R. K., Roberts, J. M., and Burkholder, J. B.: Nitryl Chloride (ClNO_2): UV/Vis Absorption Spectrum between 210 and 296 K and O(P-3) Quantum Yield at 193 and 248 nm, *J. Phys. Chem. A*, 116, 5796–5805, <https://doi.org/10.1021/jp207389y>, 2012.
- Goliff, W. S., Stockwell, W. R., and Lawson, C. V.: The regional atmospheric chemistry mechanism, version 2, *Atmos. Environ.*, 68, 174–185, <https://doi.org/10.1016/j.atmosenv.2012.11.038>, 2013.
- Hallquist, M., Stewart, D. J., Stephenson, S. K., and Cox, R. A.: Hydrolysis of N_2O_5 on sub-micron sulfate aerosols, *Phys. Chem. Chem. Phys.*, 5, 3453–3463, <https://doi.org/10.1039/B301827j>, 2003.
- Haskins, J. D., Lee, B. H., Lopez-Hilfiker, F. D., Peng, Q. Y., Jaegle, L., Reeves, J. M., Schroder, J. C., Campuzano-Jost, P., Fibiger, D., McDuffie, E. E., Jimenez, J. L., Brown, S. S., and Thornton, J. A.: Observational Constraints on the Formation of Cl_2 From the Reactive Uptake of ClNO_2 on Aerosols in the Polluted Marine Boundary Layer, *J. Geophys. Res.-Atmos.*, 124, 8851–8869, <https://doi.org/10.1029/2019jd030627>, 2019.
- He, X., Yuan, B., Wu, C., Wang, S., Wang, C., Huangfu, Y., Qi, J., Ma, N., Xu, W., Wang, M., Chen, W., Su, H., Cheng, Y., and Shao, M.: Volatile organic compounds in wintertime North China Plain: Insights from measurements of proton transfer reaction time-of-flight mass spectrometer (PTR-ToF-MS), *J. Environ. Sci.*, 114, 98–114, <https://doi.org/10.1016/j.jes.2021.08.010>, 2022.
- Jeong, D., Seco, R., Gu, D., Lee, Y., Nault, B. A., Knote, C. J., Mcgee, T., Sullivan, J. T., Jimenez, J. L., Campuzano-Jost, P., Blake, D. R., Sanchez, D., Guenther, A. B., Tanner, D., Huey, L. G., Long, R., Anderson, B. E., Hall, S. R., Ullmann, K., Shin, H., Herndon, S. C., Lee, Y., Kim, D., Ahn, J., and Kim, S.: Integration of airborne and ground observations of nitryl chloride in the Seoul metropolitan area and the implications on regional oxidation capacity during KORUS-AQ 2016, *Atmos. Chem. Phys.*, 19, 12779–12795, <https://doi.org/10.5194/acp-19-12779-2019>, 2019.
- Le Breton, M., Hallquist, Å. M., Pathak, R. K., Simpson, D., Wang, Y., Johansson, J., Zheng, J., Yang, Y., Shang, D., Wang, H., Liu, Q., Chan, C., Wang, T., Bannan, T. J., Priestley, M., Percival, C. J., Shallcross, D. E., Lu, K., Guo, S., Hu, M., and Hallquist, M.: Chlorine oxidation of VOCs at a semi-rural site in Beijing: significant chlorine liberation from ClNO_2 and subsequent gas- and particle-phase Cl -VOC production, *Atmos. Chem. Phys.*, 18, 13013–13030, <https://doi.org/10.5194/acp-18-13013-2018>, 2018.
- Li, Q., Fu, X., Peng, X., Wang, W., Badia, A., Fernandez, R. P., Cuevas, C. A., Mu, Y., Chen, J., Jimenez, J. L., Wang, T., and Saiz-Lopez, A.: Halogens Enhance Haze Pollution in China, *Environ. Sci. Technol.*, 55, 13625–13637, <https://doi.org/10.1021/acs.est.1c01949>, 2021.
- Li, Q., Zhang, L., Wang, T., Tham, Y. J., Ahmadov, R., Xue, L., Zhang, Q., and Zheng, J.: Impacts of heterogeneous uptake of dinitrogen pentoxide and chlorine activation on ozone and reactive nitrogen partitioning: improvement and application of the WRF-Chem model in southern China, *Atmos. Chem. Phys.*, 16, 14875–14890, <https://doi.org/10.5194/acp-16-14875-2016>, 2016.
- Li, Q., Borge, R., Sarwar, G., de la Paz, D., Gantt, B., Domingo, J., Cuevas, C. A., and Saiz-Lopez, A.: Impact of halogen chemistry on summertime air quality in coastal and continental Europe: application of the CMAQ model and implications for regulation, *Atmos. Chem. Phys.*, 19, 15321–15337, <https://doi.org/10.5194/acp-19-15321-2019>, 2019.

- Liu, X. G., Gu, J. W., Li, Y. P., Cheng, Y. F., Qu, Y., Han, T. T., Wang, J. L., Tian, H. Z., Chen, J., and Zhang, Y. H.: Increase of aerosol scattering by hygroscopic growth: Observation, modeling, and implications on visibility, *Atmos. Res.*, 132, 91–101, <https://doi.org/10.1016/j.atmosres.2013.04.007>, 2013.
- Liu, X. X., Qu, H., Huey, L. G., Wang, Y. H., Sjostedt, S., Zeng, L. M., Lu, K. D., Wu, Y. S., Ho, M., Shao, M., Zhu, T., and Zhang, Y. H.: High Levels of Daytime Molecular Chlorine and Nitryl Chloride at a Rural Site on the North China Plain, *Environ. Sci. Technol.*, 51, 9588–9595, <https://doi.org/10.1021/acs.est.7b03039>, 2017.
- Lou, S., Tan, Z., Gan, G., Chen, J., Wang, H., Gao, Y., Huang, D., Huang, C., Li, X., Song, R., Wang, H., Wang, M., Wang, Q., Wu, Y., and Huang, C.: Observation based study on atmospheric oxidation capacity in Shanghai during late-autumn: Contribution from nitryl chloride, *Atmos. Environ.*, 271, 118902, <https://doi.org/10.1016/j.atmosenv.2021.118902>, 2022.
- Lu, K. D., Rohrer, F., Holland, F., Fuchs, H., Bohn, B., Brauers, T., Chang, C. C., Häseler, R., Hu, M., Kita, K., Kondo, Y., Li, X., Lou, S. R., Nehr, S., Shao, M., Zeng, L. M., Wahner, A., Zhang, Y. H., and Hofzumahaus, A.: Observation and modelling of OH and HO₂ concentrations in the Pearl River Delta 2006: a missing OH source in a VOC rich atmosphere, *Atmos. Chem. Phys.*, 12, 1541–1569, <https://doi.org/10.5194/acp-12-1541-2012>, 2012.
- McDuffie, E. E., Fibiger, D. L., Dube, W. P., Hilfiker, F. L., Lee, B. H., Jaegle, L., Guo, H. Y., Weber, R. J., Reeves, J. M., Weinheimer, A. J., Schroder, J. C., Campuzano-Jost, P., Jimenez, J. L., Dibb, J. E., Veres, P., Ebben, C., Sparks, T. L., Wooldridge, P. J., Cohen, R. C., Campos, T., Hall, S. R., Ullmann, K., Roberts, J. M., Thornton, J. A., and Brown, S. S.: ClNO₂ Yields From Aircraft Measurements During the 2015 WINTER Campaign and Critical Evaluation of the Current Parameterization, *J. Geophys. Res.-Atmos.*, 123, 12994–13015, <https://doi.org/10.1029/2018JD029358>, 2018a.
- McDuffie, E. E., Fibiger, D. L., Dube, W. P., Lopez-Hilfiker, F., Lee, B. H., Thornton, J. A., Shah, V., Jaegle, L., Guo, H. Y., Weber, R. J., Reeves, J. M., Weinheimer, A. J., Schroder, J. C., Campuzano-Jost, P., Jimenez, J. L., Dibb, J. E., Veres, P., Ebben, C., Sparks, T. L., Wooldridge, P. J., Cohen, R. C., Hornbrook, R. S., Apel, E. C., Campos, T., Hall, S. R., Ullmann, K., and Brown, S. S.: Heterogeneous N₂O₅ Uptake During Winter: Aircraft Measurements During the 2015 WINTER Campaign and Critical Evaluation of Current Parameterizations, *J. Geophys. Res.-Atmos.*, 123, 4345–4372, <https://doi.org/10.1002/2018jd028336>, 2018b.
- Mentel, T. F., Sohn, M., and Wahner, A.: Nitrate effect in the heterogeneous hydrolysis of dinitrogen pentoxide on aqueous aerosols, *Phys. Chem. Chem. Phys.*, 1, 5451–5457, <https://doi.org/10.1039/A905338g>, 1999.
- Mielke, L. H., Stutz, J., Tsai, C., Hurlock, S. C., Roberts, J. M., Veres, P. R., Froyd, K. D., Hayes, P. L., Cubison, M. J., Jimenez, J. L., Washenfelder, R. A., Young, C. J., Gilman, J. B., de Gouw, J. A., Flynn, J. H., Grossberg, N., Lefer, B. L., Liu, J., Weber, R. J., and Osthoff, H. D.: Heterogeneous formation of nitryl chloride and its role as a nocturnal NO_x reservoir species during CalNex-LA 2010, *J. Geophys. Res.-Atmos.*, 118, 10638–10652, <https://doi.org/10.1002/Jgrd.50783>, 2013.
- Mielke, L. H., Furgeson, A., Odam-Ankrah, C. A., and Osthoff, H. D.: Ubiquity of ClNO₂ in the urban boundary layer of Calgary, Alberta, Canada, *Can. J. Chem.*, 94, 414–423, <https://doi.org/10.1139/cjc-2015-0426>, 2015.
- Mozurkewich, M. and Calvert, J. G.: Reaction Probability of N₂O₅ on Aqueous Aerosols, *J. Geophys. Res.-Atmos.*, 93, 15889–15896, <https://doi.org/10.1029/JD093iD12p15889>, 1988.
- Osthoff, H. D., Roberts, J. M., Ravishankara, A. R., Williams, E. J., Lerner, B. M., Sommariva, R., Bates, T. S., Coffman, D., Quinn, P. K., Dibb, J. E., Stark, H., Burkholder, J. B., Talukdar, R. K., Meagher, J., Fehsenfeld, F. C., and Brown, S. S.: High levels of nitryl chloride in the polluted subtropical marine boundary layer, *Nat. Geosci.*, 1, 324–328, <https://doi.org/10.1038/Ngeo177>, 2008.
- Peng, X., Wang, W., Xia, M., Chen, H., Ravishankara, A. R., Li, Q., Saiz-Lopez, A., Liu, P., Zhang, F., Zhang, C., Xue, L., Wang, X., George, C., Wang, J., Mu, Y., Chen, J., and Wang, T.: An unexpected large continental source of reactive bromine and chlorine with significant impact on wintertime air quality, *Natl. Sci. Rev.*, 8, nwaa304, <https://doi.org/10.1093/nsr/nwaa304>, 2021.
- Phillips, G. J., Tang, M. J., Thieser, J., Brickwedde, B., Schuster, G., Bohn, B., Lelieveld, J., and Crowley, J. N.: Significant concentrations of nitryl chloride observed in rural continental Europe associated with the influence of sea salt chloride and anthropogenic emissions, *Geophys. Res. Lett.*, 39, L10811, <https://doi.org/10.1029/2012gl051912>, 2012.
- Phillips, G. J., Thieser, J., Tang, M., Sobanski, N., Schuster, G., Fachinger, J., Drewnick, F., Borrmann, S., Bingemer, H., Lelieveld, J., and Crowley, J. N.: Estimating N₂O₅ uptake coefficients using ambient measurements of NO₃, N₂O₅, ClNO₂ and particle-phase nitrate, *Atmos. Chem. Phys.*, 16, 13231–13249, <https://doi.org/10.5194/acp-16-13231-2016>, 2016.
- Riedel, T. P., Bertram, T. H., Crisp, T. A., Williams, E. J., Lerner, B. M., Vlasenko, A., Li, S. M., Gilman, J., de Gouw, J., Bon, D. M., Wagner, N. L., Brown, S. S., and Thornton, J. A.: Nitryl Chloride and Molecular Chlorine in the Coastal Marine Boundary Layer, *Environ. Sci. Technol.*, 46, 10463–10470, <https://doi.org/10.1021/es204632r>, 2012.
- Riedel, T. P., Wagner, N. L., Dube, W. P., Middlebrook, A. M., Young, C. J., Ozturk, F., Bahreini, R., VandenBoer, T. C., Wolfe, D. E., Williams, E. J., Roberts, J. M., Brown, S. S., and Thornton, J. A.: Chlorine activation within urban or power plant plumes: Vertically resolved ClNO₂ and Cl₂ measurements from a tall tower in a polluted continental setting, *J. Geophys. Res.-Atmos.*, 118, 8702–8715, <https://doi.org/10.1002/jgrd.50637>, 2013.
- Riedel, T. P., Wolfe, G. M., Danas, K. T., Gilman, J. B., Kuster, W. C., Bon, D. M., Vlasenko, A., Li, S.-M., Williams, E. J., Lerner, B. M., Veres, P. R., Roberts, J. M., Holloway, J. S., Lefer, B., Brown, S. S., and Thornton, J. A.: An MCM modeling study of nitryl chloride (ClNO₂) impacts on oxidation, ozone production and nitrogen oxide partitioning in polluted continental outflow, *Atmos. Chem. Phys.*, 14, 3789–3800, <https://doi.org/10.5194/acp-14-3789-2014>, 2014.
- Roberts, J. M., Osthoff, H. D., Brown, S. S., Ravishankara, A. R., Coffman, D., Quinn, P., and Bates, T.: Laboratory studies of products of N₂O₅ uptake on Cl-containing substrates, *Geophys. Res. Lett.*, 36, L20808, <https://doi.org/10.1029/2009gl040448>, 2009.
- Ryder, O. S., Campbell, N. R., Shalowski, M., Al-Mashat, H., Nathanson, G. M., and Bertram, T. H.: Role of Organics in Regu-

- lating ClNO₂ Production at the Air-Sea Interface, *J. Phys. Chem. A*, 119, 8519–8526, <https://doi.org/10.1021/jp5129673>, 2015.
- Saiz-Lopez, A. and von Glasow, R.: Reactive halogen chemistry in the troposphere, *Chem. Soc. Rev.*, 41, 6448–6472, 2012.
- Sarwar, G., Simon, H., Xing, J., and Mathur, R.: Importance of tropospheric ClNO₂ chemistry across the Northern Hemisphere, *Geophys. Res. Lett.*, 41, 4050–4058, <https://doi.org/10.1002/2014gl059962>, 2014.
- Shi, B., Wang, W., Zhou, L., Sun, Z., Fan, C., Chen, Y., Zhang, W., Qiao, Y., Qiao, Y., and Ge, M.: Atmospheric oxidation of C₁₀–14 n-alkanes initiated by Cl atoms: Kinetics and mechanism, *Atmos. Environ.*, 222, 117166, <https://doi.org/10.1016/j.atmosenv.2019.117166>, 2020.
- Simpson, W. R., Brown, S. S., Saiz-Lopez, A., Thornton, J. A., and von Glasow, R.: Tropospheric Halogen Chemistry: Sources, Cycling, and Impacts, *Chem. Rev.*, 115, 4035–4062, <https://doi.org/10.1021/cr5006638>, 2015.
- Sommariva, R., Hollis, L. D. J., Sherwen, T., Baker, A. R., Ball, S. M., Bandy, B. J., Bell, T. G., Chowdhury, M. N., Cordell, R. L., Evans, M. J., Lee, J. D., Reed, C., Reeves, C. E., Roberts, J. M., Yang, M. X., and Monks, P. S.: Seasonal and geographical variability of nitryl chloride and its precursors in Northern Europe, *Atmos. Sci. Lett.*, 19, UNSP e844, <https://doi.org/10.1002/asl.844>, 2018.
- Staudt, S., Gord, J. R., Karimova, N. V., McDuffie, E. E., Brown, S. S., Gerber, R. B., Nathanson, G. M., and Bertram, T. H.: Sulfate and Carboxylate Suppress the Formation of ClNO₂ at Atmospheric Interfaces, *ACS Earth Space Chem.*, 3, 1987–1997, <https://doi.org/10.1021/acsearthspacechem.9b00177>, 2019.
- Tan, Z., Fuchs, H., Lu, K., Hofzumahaus, A., Bohn, B., Broch, S., Dong, H., Gomm, S., Häseler, R., He, L., Holland, F., Li, X., Liu, Y., Lu, S., Rohrer, F., Shao, M., Wang, B., Wang, M., Wu, Y., Zeng, L., Zhang, Y., Wahner, A., and Zhang, Y.: Radical chemistry at a rural site (Wangdu) in the North China Plain: observation and model calculations of OH, HO₂ and RO₂ radicals, *Atmos. Chem. Phys.*, 17, 663–690, <https://doi.org/10.5194/acp-17-663-2017>, 2017.
- Tan, Z., Lu, K., Hofzumahaus, A., Fuchs, H., Bohn, B., Holland, F., Liu, Y., Rohrer, F., Shao, M., Sun, K., Wu, Y., Zeng, L., Zhang, Y., Zou, Q., Kiendler-Scharr, A., Wahner, A., and Zhang, Y.: Experimental budgets of OH, HO₂, and RO₂ radicals and implications for ozone formation in the Pearl River Delta in China 2014, *Atmos. Chem. Phys.*, 19, 7129–7150, <https://doi.org/10.5194/acp-19-7129-2019>, 2019.
- Tang, M. J., Telford, P. J., Pope, F. D., Rkiouak, L., Abraham, N. L., Archibald, A. T., Braesicke, P., Pyle, J. A., McGregor, J., Watson, I. M., Cox, R. A., and Kalberer, M.: Heterogeneous reaction of N₂O₅ with airborne TiO₂ particles and its implication for stratospheric particle injection, *Atmos. Chem. Phys.*, 14, 6035–6048, <https://doi.org/10.5194/acp-14-6035-2014>, 2014.
- Thaler, R. D., Mielke, L. H., and Osthoff, H. D.: Quantification of Nitryl Chloride at Part Per Trillion Mixing Ratios by Thermal Dissociation Cavity Ring-Down Spectroscopy, *Anal. Chem.*, 83, 2761–2766, <https://doi.org/10.1021/ac200055z>, 2011.
- Tham, Y. J., Yan, C., Xue, L. K., Zha, Q. Z., Wang, X. F., and Wang, T.: Presence of high nitryl chloride in Asian coastal environment and its impact on atmospheric photochemistry, *Chinese Sci. Bull.*, 59, 356–359, <https://doi.org/10.1007/s11434-013-0063-y>, 2014.
- Tham, Y. J., Wang, Z., Li, Q., Yun, H., Wang, W., Wang, X., Xue, L., Lu, K., Ma, N., Bohn, B., Li, X., Kecorius, S., Groß, J., Shao, M., Wiedensohler, A., Zhang, Y., and Wang, T.: Significant concentrations of nitryl chloride sustained in the morning: investigations of the causes and impacts on ozone production in a polluted region of northern China, *Atmos. Chem. Phys.*, 16, 14959–14977, <https://doi.org/10.5194/acp-16-14959-2016>, 2016.
- Tham, Y. J., Wang, Z., Li, Q., Wang, W., Wang, X., Lu, K., Ma, N., Yan, C., Kecorius, S., Wiedensohler, A., Zhang, Y., and Wang, T.: Heterogeneous N₂O₅ uptake coefficient and production yield of ClNO₂ in polluted northern China: roles of aerosol water content and chemical composition, *Atmos. Chem. Phys.*, 18, 13155–13171, <https://doi.org/10.5194/acp-18-13155-2018>, 2018.
- Thornton, J. A., Kercher, J. P., Riedel, T. P., Wagner, N. L., Cozic, J., Holloway, J. S., Dube, W. P., Wolfe, G. M., Quinn, P. K., Middlebrook, A. M., Alexander, B., and Brown, S. S.: A large atomic chlorine source inferred from mid-continental reactive nitrogen chemistry, *Nature*, 464, 271–274, <https://doi.org/10.1038/nature08905>, 2010.
- Veres, P. R., Neuman, J. A., Bertram, T. H., Assaf, E., Wolfe, G. M., Williamson, C. J., Weinzierl, B., Tilmes, S., Thompson, C. R., Thames, A. B., Schroder, J. C., Saiz-Lopez, A., Rollins, A. W., Roberts, J. M., Price, D., Peischl, J., Nault, B. A., Moller, K. H., Miller, D. O., Meinardi, S., Li, Q., Lamarque, J. F., Kupc, A., Kjaergaard, H. G., Kinnison, D., Jimenez, J. L., Jernigan, C. M., Hornbrook, R. S., Hills, A., Dollner, M., Day, D. A., Cuevas, C. A., Campuzano-Jost, P., Burkholder, J., Bui, T. P., Brune, W. H., Brown, S. S., Brock, C. A., Bourgeois, I., Blake, D. R., Apel, E. C., and Ryerson, T. B.: Global airborne sampling reveals a previously unobserved dimethyl sulfide oxidation mechanism in the marine atmosphere, *P. Natl. Acad. Sci. USA*, 117, 4505–4510, <https://doi.org/10.1073/pnas.1919344117>, 2020.
- Wagner, N. L., Riedel, T. P., Roberts, J. M., Thornton, J. A., Angevine, W. M., Williams, E. J., Lerner, B. M., Vlasenko, A., Li, S. M., Dube, W. P., Coffman, D. J., Bon, D. M., de Gouw, J. A., Kuster, W. C., Gilman, J. B., and Brown, S. S.: The sea breeze/land breeze circulation in Los Angeles and its influence on nitryl chloride production in this region, *J. Geophys. Res.-Atmos.*, 117, D00v24, <https://doi.org/10.1029/2012jd017810>, 2012.
- Wahner, A., Mentel, T. F., Sohn, M., and Stier, J.: Heterogeneous reaction of N₂O₅ on sodium nitrate aerosol, *J. Geophys. Res.-Atmos.*, 103, 31103–31112, <https://doi.org/10.1029/1998jd100022>, 1998.
- Wang, H. and Lu, K.: Monitoring Ambient Nitrate Radical by Open-Path Cavity-Enhanced Absorption Spectroscopy, *Anal. Chem.*, 91, 10687–10693, <https://doi.org/10.1021/acs.analchem.9b01971>, 2019.
- Wang, H., Lu, K., Chen, X., Zhu, Q., Chen, Q., Guo, S., Jiang, M., Li, X., Shang, D., Tan, Z., Wu, Y., Wu, Z., Zou, Q., Zheng, Y., Zeng, L., Zhu, T., Hu, M., and Zhang, Y.: High N₂O₅ Concentrations Observed in Urban Beijing: Implications of a Large Nitrate Formation Pathway, *Environ. Sci. Technol. Lett.*, 4, 416–420, <https://doi.org/10.1021/acs.estlett.7b00341>, 2017a.
- Wang, H., Lu, K., Tan, Z., Sun, K., Li, X., Hu, M., Shao, M., Zeng, L., Zhu, T., and Zhang, Y.: Model simulation of NO₃, N₂O₅ and ClNO₂ at a rural site in Beijing during CAREBeijing-2006, *Atmos. Res.*, 196, 97–107, <https://doi.org/10.1016/j.atmosres.2017.06.013>, 2017b.

- Wang, H., Lu, K., Guo, S., Wu, Z., Shang, D., Tan, Z., Wang, Y., Le Breton, M., Lou, S., Tang, M., Wu, Y., Zhu, W., Zheng, J., Zeng, L., Hallquist, M., Hu, M., and Zhang, Y.: Efficient N_2O_5 uptake and NO_3 oxidation in the outflow of urban Beijing, *Atmos. Chem. Phys.*, 18, 9705–9721, <https://doi.org/10.5194/acp-18-9705-2018>, 2018.
- Wang, H., Chen, X., Lu, K., Tan, Z., Ma, X., Wu, Z., Li, X., Liu, Y., Shang, D., Wu, Y., Zeng, L., Hu, M., Schmitt, S., Kiendler-Scharr, A., Wahner, A., and Zhang, Y.: Wintertime N_2O_5 uptake coefficients over the North China Plain, *Sci. Bull.*, 65, 765–774, <https://doi.org/10.1016/j.scib.2020.02.006>, 2020.
- Wang, H., Peng, C., Wang, X., Lou, S., Lu, K., Gan, G., Jia, X., Chen, X., Chen, J., Wang, H., Fan, S., Wang, X., and Tang, M.: N_2O_5 uptake onto saline mineral dust: a potential missing source of tropospheric ClNO_2 in inland China, *Atmos. Chem. Phys.*, 22, 1845–1859, <https://doi.org/10.5194/acp-22-1845-2022>, 2022.
- Wang, K., Wang, W., Fan, C., Li, J., Lei, T., Zhang, W., Shi, B., Chen, Y., Liu, M., Lian, C., Wang, Z., and Ge, M.: Reactions of C_{12} – C_{14} n-Alkylcyclohexanes with Cl Atoms: Kinetics and Secondary Organic Aerosol Formation, *Environ. Sci. Technol.*, 56, 4859–4870, <https://doi.org/10.1021/acs.est.1c08958>, 2022.
- Wang, T., Tham, Y. J., Xue, L. K., Li, Q. Y., Zha, Q. Z., Wang, Z., Poon, S. C. N., Dube, W. P., Blake, D. R., Louie, P. K. K., Luk, C. W. Y., Tsui, W., and Brown, S. S.: Observations of nitryl chloride and modeling its source and effect on ozone in the planetary boundary layer of southern China, *J. Geophys. Res.-Atmos.*, 121, 2476–2489, <https://doi.org/10.1002/2015jd024556>, 2016.
- Wang, T., Dai, J. N., Lam, K. S., Poon, C. N., and Brasseur, G. P.: Twenty-Five Years of Lower Tropospheric Ozone Observations in Tropical East Asia: The Influence of Emissions and Weather Patterns, *Geophys. Res. Lett.*, 46, 11463–11470, <https://doi.org/10.1029/2019gl084459>, 2019.
- Wang, W., Yuan, B., Peng, Y., Su, H., Cheng, Y., Yang, S., Wu, C., Qi, J., Bao, F., Huangfu, Y., Wang, C., Ye, C., Wang, Z., Wang, B., Wang, X., Song, W., Hu, W., Cheng, P., Zhu, M., Zheng, J., and Shao, M.: Direct observations indicate photodegradable oxygenated volatile organic compounds (OVOCs) as larger contributors to radicals and ozone production in the atmosphere, *Atmos. Chem. Phys.*, 22, 4117–4128, <https://doi.org/10.5194/acp-22-4117-2022>, 2022.
- Wang, X., Jacob, D. J., Eastham, S. D., Sulprizio, M. P., Zhu, L., Chen, Q., Alexander, B., Sherwen, T., Evans, M. J., Lee, B. H., Haskins, J. D., Lopez-Hilfiker, F. D., Thornton, J. A., Huey, G. L., and Liao, H.: The role of chlorine in global tropospheric chemistry, *Atmos. Chem. Phys.*, 19, 3981–4003, <https://doi.org/10.5194/acp-19-3981-2019>, 2019.
- Wang, X. F., Wang, H., Xue, L. K., Wang, T., Wang, L. W., Gu, R. R., Wang, W. H., Tham, Y. J., Wang, Z., Yang, L. X., Chen, J. M., and Wang, W. X.: Observations of N_2O_5 and ClNO_2 at a polluted urban surface site in North China: High N_2O_5 uptake coefficients and low ClNO_2 product yields, *Atmos. Environ.*, 156, 125–134, <https://doi.org/10.1016/j.atmosenv.2017.02.035>, 2017.
- Wang, Z., Wang, W., Tham, Y. J., Li, Q., Wang, H., Wen, L., Wang, X., and Wang, T.: Fast heterogeneous N_2O_5 uptake and ClNO_2 production in power plant and industrial plumes observed in the nocturnal residual layer over the North China Plain, *Atmos. Chem. Phys.*, 17, 12361–12378, <https://doi.org/10.5194/acp-17-12361-2017>, 2017.
- Wang, Z., Yuan, B., Ye, C., Roberts, J., Wisthaler, A., Lin, Y., Li, T., Wu, C., Peng, Y., Wang, C., Wang, S., Yang, S., Wang, B., Qi, J., Wang, C., Song, W., Hu, W., Wang, X., Xu, W., Ma, N., Kuang, Y., Tao, J., Zhang, Z., Su, H., Cheng, Y., Wang, X., and Shao, M.: High Concentrations of Atmospheric Isocyanic Acid (HNCO) Produced from Secondary Sources in China, *Environ. Sci. Technol.*, 54, 11818–11826, <https://doi.org/10.1021/acs.est.0c02843>, 2020.
- Wu, C., Wang, C., Wang, S., Wang, W., Yuan, B., Qi, J., Wang, B., Wang, H., Wang, C., Song, W., Wang, X., Hu, W., Lou, S., Ye, C., Peng, Y., Wang, Z., Huangfu, Y., Xie, Y., Zhu, M., Zheng, J., Wang, X., Jiang, B., Zhang, Z., and Shao, M.: Measurement report: Important contributions of oxygenated compounds to emissions and chemistry of volatile organic compounds in urban air, *Atmos. Chem. Phys.*, 20, 14769–14785, <https://doi.org/10.5194/acp-20-14769-2020>, 2020.
- Xia, M., Peng, X., Wang, W., Yu, C., Sun, P., Li, Y., Liu, Y., Xu, Z., Wang, Z., Xu, Z., Nie, W., Ding, A., and Wang, T.: Significant production of ClNO_2 and possible source of Cl_2 from N_2O_5 uptake at a suburban site in eastern China, *Atmos. Chem. Phys.*, 20, 6147–6158, <https://doi.org/10.5194/acp-20-6147-2020>, 2020.
- Xia, M., Peng, X., Wang, W., Yu, C., Wang, Z., Tham, Y. J., Chen, J., Chen, H., Mu, Y., Zhang, C., Liu, P., Xue, L., Wang, X., Gao, J., Li, H., and Wang, T.: Winter ClNO_2 formation in the region of fresh anthropogenic emissions: seasonal variability and insights into daytime peaks in northern China, *Atmos. Chem. Phys.*, 21, 15985–16000, <https://doi.org/10.5194/acp-21-15985-2021>, 2021.
- Xue, L. K., Saunders, S. M., Wang, T., Gao, R., Wang, X. F., Zhang, Q. Z., and Wang, W. X.: Development of a chlorine chemistry module for the Master Chemical Mechanism, *Geosci. Model Dev.*, 8, 3151–3162, <https://doi.org/10.5194/gmd-8-3151-2015>, 2015.
- Yang, S., Yuan, B., Peng, Y., Huang, S., Chen, W., Hu, W., Pei, C., Zhou, J., Parrish, D. D., Wang, W., He, X., Cheng, C., Li, X.-B., Yang, X., Song, Y., Wang, H., Qi, J., Wang, B., Wang, C., Wang, C., Wang, Z., Li, T., Zheng, E., Wang, S., Wu, C., Cai, M., Ye, C., Song, W., Cheng, P., Chen, D., Wang, X., Zhang, Z., Wang, X., Zheng, J., and Shao, M.: The formation and mitigation of nitrate pollution: comparison between urban and suburban environments, *Atmos. Chem. Phys.*, 22, 4539–4556, <https://doi.org/10.5194/acp-22-4539-2022>, 2022.
- Yang, X., Wang, T., Xia, M., Gao, X. M., Li, Q. Y., Zhang, N. W., Gao, Y., Lee, S. C., Wang, X. F., Xue, L. K., Yang, L. X., and Wang, W. X.: Abundance and origin of fine particulate chloride in continental China, *Sci. Total Environ.*, 624, 1041–1051, <https://doi.org/10.1016/j.scitotenv.2017.12.205>, 2018.
- Yang, X., Wang, Q., Ma, N., Hu, W., Gao, Y., Huang, Z., Zheng, J., Yuan, B., Yang, N., Tao, J., Hong, J., Cheng, Y., and Su, H.: The impact of chlorine chemistry combined with heterogeneous N_2O_5 reactions on air quality in China, *Atmos. Chem. Phys.*, 22, 3743–3762, <https://doi.org/10.5194/acp-22-3743-2022>, 2022.
- Ye, C., Yuan, B., Lin, Y., Wang, Z., Hu, W., Li, T., Chen, W., Wu, C., Wang, C., Huang, S., Qi, J., Wang, B., Wang, C., Song, W., Wang, X., Zheng, E., Krechmer, J. E., Ye, P., Zhang, Z., Wang, X., Worsnop, D. R., and Shao, M.: Chemical characterization of oxygenated organic compounds in the gas phase and particle phase using iodide CIMS with FIGAERO in urban air, *At-*

- mos. Chem. Phys., 21, 8455–8478, <https://doi.org/10.5194/acp-21-8455-2021>, 2021.
- Young, C. J., Washenfelder, R. A., Roberts, J. M., Mielke, L. H., Osthoff, H. D., Tsai, C., Pikel'naya, O., Stutz, J., Veres, P. R., Cochran, A. K., VandenBoer, T. C., Flynn, J., Grossberg, N., Haman, C. L., Lefer, B., Stark, H., Graus, M., de Gouw, J., Gilman, J. B., Kuster, W. C., and Brown, S. S.: Vertically Resolved Measurements of Nighttime Radical Reservoirs; in Los Angeles and Their Contribution to the Urban Radical Budget, *Environ. Sci. Technol.*, 46, 10965–10973, <https://doi.org/10.1021/es302206a>, 2012.
- Yu, C., Wang, Z., Xia, M., Fu, X., Wang, W., Tham, Y. J., Chen, T., Zheng, P., Li, H., Shan, Y., Wang, X., Xue, L., Zhou, Y., Yue, D., Ou, Y., Gao, J., Lu, K., Brown, S. S., Zhang, Y., and Wang, T.: Heterogeneous N_2O_5 reactions on atmospheric aerosols at four Chinese sites: improving model representation of uptake parameters, *Atmos. Chem. Phys.*, 20, 4367–4378, <https://doi.org/10.5194/acp-20-4367-2020>, 2020.
- Yun, H., Wang, T., Wang, W. H., Tham, Y. J., Li, Q. Y., Wang, Z., and Poon, S. C. N.: Nighttime NO_x loss and ClNO_2 formation in the residual layer of a polluted region: Insights from field measurements and an iterative box model, *Sci. Total Environ.*, 622, 727–734, <https://doi.org/10.1016/j.scitotenv.2017.11.352>, 2018a.
- Yun, H., Wang, W., Wang, T., Xia, M., Yu, C., Wang, Z., Poon, S. C. N., Yue, D., and Zhou, Y.: Nitrate formation from heterogeneous uptake of dinitrogen pentoxide during a severe winter haze in southern China, *Atmos. Chem. Phys.*, 18, 17515–17527, <https://doi.org/10.5194/acp-18-17515-2018>, 2018b.
- Zhou, W., Zhao, J., Ouyang, B., Mehra, A., Xu, W., Wang, Y., Bannan, T. J., Worrall, S. D., Priestley, M., Bacak, A., Chen, Q., Xie, C., Wang, Q., Wang, J., Du, W., Zhang, Y., Ge, X., Ye, P., Lee, J. D., Fu, P., Wang, Z., Worsnop, D., Jones, R., Percival, C. J., Coe, H., and Sun, Y.: Production of N_2O_5 and ClNO_2 in summer in urban Beijing, China, *Atmos. Chem. Phys.*, 18, 11581–11597, <https://doi.org/10.5194/acp-18-11581-2018>, 2018.
- Zong, T., Wang, H., Wu, Z., Lu, K., Wang, Y., Zhu, Y., Shang, D., Fang, X., Huang, X., He, L., Ma, N., Gross, J., Huang, S., Guo, S., Zeng, L., Herrmann, H., Wiedensohler, A., Zhang, Y., and Hu, M.: Particle hygroscopicity inhomogeneity and its impact on reactive uptake, *Sci. Total Environ.*, 151364–151364, <https://doi.org/10.1016/j.scitotenv.2021.151364>, 2021.